

Implementation of Kalmus' guidance method for robot navigation

by

Kostiantyn Gorbatov

BEng (Hons) Robotics & Automated Systems 2016

A report submitted to the University of Plymouth

In partial fulfilment for the degree of

BEng(Hons) Robotics and Automated Systems

FACULTY of SCIENCE & TECHNOLOGY

UNIVERSITY of PLYMOUTH

MAY 2016

Summary

The principle of operation of a position and orientation inductive sensor is based on a detailed mapping of quasistatic magnetic fields induced in free space by a set of miniature coils (or loops) called “magnetic dipoles”. Depending on the task, one, two or a maximum of three coils in the mutually orthogonal planes can be used to produce the required magnetic pattern in free space. Each coil is energised by a sinusoidal current in the kHz range or a pulse sequence: independently or with a certain phase. The quasistatic condition means that the electromagnetic wavelength in free space is much larger than any dimensions in the system, including the coil diameters and the distance between the source of magnetic field and the sensor head. Therefore, the retardation effect caused by the finite speed of light can be completely neglected. The aim is to obtain a unique vector magnetic field (time-dependent) in each coordinate point. The magnetic field in an observation point can be measured by means of a set of miniature coils (or loops) comprising the sensor head which is attached to the tracking object. The sensor head may also include one, two, or a maximum of three miniature coils in the mutually orthogonal planes. To recognise the position and orientation of the sensor head, some algorithm has to be proposed that recalculates the magnetic field pattern into the coordinates and orientation angles.

In this project, the Kalmus’ guidance method has been successfully implemented for robot navigation. The method, first proposed by Henry Kalmus^{*)}, was originally designed to aid vehicles to follow one another. In his method, the two crossed excitation coils are fed from a low frequency source (kHz) in phase quadrature ($\pi/2$ -phase shift). The sensor head placed on a moving platform comprises the two crossed pickup coils and changes its azimuthal orientation with respect to the line of sight between the excitation and sensor heads. It has been shown that the orientation can be determined by measuring the phase difference between the pickup voltages. I used this principle to build a navigation system that forces the slave mobile platform (“tank”) to follow the leading platform. The leading platform is controlled using remote control and carries the transmission coils (source of quasistatic magnetic field), while the slave platform carries the pickup coils that provide information on the distance from the source of magnetic field and its angle position with respect to the slave platform. Based on a short research, this is the first use of inductive sensors for robot navigation. To adapt the Kalmus’ guidance method, modern electronic components and digital signal processing techniques has been used.

^{*)} H. P. Kalmus, “A New Guiding and Tracking System”, IRE Transactions on Aerospace and Navigational Electronics, Vol. 9, pp. 7–10, (1962).

ACKNOWLEDGEMENTS

I would like to thank the following people for all their help throughout the project:

Prof. Genhua Pan, project supervisor,

Dr. Phil Culverhouse, second project supervisor

John Eastment and Sheila Storm, technicians at the project laboratory in Smeaton Building.

Contents

1. GLOSSARY	5
2. INTRODUCTION	6
3. ADAPTATION OF KALMUS' GUIDANCE METHOD FOR SPECIFIC APPLICATION.....	10
3.1 Kalmus' guidance algorithm.....	10
3.2 Design strategy of excitation coils	14
3.3 Design strategy of pickup coils	15
4. PROJECT STAGES	18
5. BUSINESS CASE RESEARCH.....	20
6. DESIGN SPECIFICATION.....	21
6.1 Fabrication of the excitation and pickup coils.....	21
6.2 Design of the transmitter electronic circuit	23
6.3 Design of the Power and Tuning stage circuit	25
6.4 Design of the filter circuit.....	28
6.5 Design of the comparator circuit.....	30
6.6. Controller circuit	32
6.6.1 Hardware specification.....	32
6.6.2 Software design	36
7. ASSEMBLY AND TESTING	41
7.1 Testing methods.....	41
7.2 Excitation circuit testing	42
7.3 Power and Input circuit testing	44
7.4 Filter circuit testing.....	47
7.5 Comparator circuit testing.....	50
7.6 Controller circuit testing.....	51
7.6.1 Hardware testing	51
7.6.2 Software testing	59
8. CONCLUSIONS.....	61
9. REFERENCES.....	62
10. APPENDICES.....	63
10.1 APPENDIX 1: Mechanical drawings for components.....	64
10. 2 APPENDIX 2: Full sized circuit diagrams.....	67
10. 3 APPENDIX 3: Datasheets.....	70
10. 4 APPENDIX 4: Project materials and cost full graph	76

1. GLOSSARY

GPIO – General purpose Input/Output pin

GPS – Global Positioning System

FPGA – Field Programmable Gate Array

ADC – Analog To Digital converter

PWM – Pulse Width Modulation

PCB – Printed circuit board

IR – Infra Red

TOF – Time of Light

WiFi – “Wireless Fidelity” (a wireless local area network protocol)

AOF – Angle of Arrival

FP – Fingerprinting

RSSI – Received Signal strength Indicator

e.m.f. – electromotive force

2. INTRODUCTION

Inductive sensors are based on a simple physical principle – Faraday's law.[1] However, the vector nature of electromagnetic field leads to rather cumbersome calculations if there is a need to predict the voltage response in a pickup coil having an arbitrary orientation. The ultimate goal is to formulate an algorithm for determining the position and orientation of a sensor head. The know-how of such sensors consists mainly in their hardware implementation. It is here that commercial companies demonstrate impressive success.[2]. However, commercial solutions are often highly specialized. In practice, the need to develop specialised sensor emerges to fulfil the needs of a particular application. The interest towards inductive sensors arose in the course of work on a reliable and inexpensive navigation system where the azimuthal orientation has to be controlled.

A static solid in free space is characterised by its position and orientation. The position is associated with the coordinates of some “natural” central point of the solid, for example, its centre of gravity or symmetry. With respect to this centre, the solid can be further rotated allowing orientational freedom. Thus, in general, there are six degrees of freedom: 3 for the position and 3 for the orientation. In some applications, the tracking object may be restricted in its motion that leads to a reduced number of degrees of freedom. The principle of operation of a position and orientation inductive sensor is based on a detailed mapping of quasistatic magnetic fields induced in free space by a set of miniature coils (or loops) called “magnetic dipoles”. [2,3] Depending on the task, one, two or a maximum of three coils in the mutually orthogonal planes can be used to produce the required magnetic pattern in free space. Each coil is energised by a sinusoidal current in the kHz range or a pulse sequence: independently or with a certain phase. The quasistatic condition means that the electromagnetic wavelength in free space is much larger than any dimensions in the system, including the coil diameters and the distance between the source of magnetic field and the sensor head. Therefore, the retardation effect caused by the finite speed of light can be completely neglected. The aim is to obtain a unique vector magnetic field (time-dependent) in each coordinate point. The magnetic field in an observation point can be measured by means of a set of miniature coils (or loops) comprising the sensor head which is attached to the tracking object. The sensor head may also include one, two, or a maximum of three miniature coils in the mutually orthogonal planes. To recognise the position and orientation of the sensor head, some algorithm has to be proposed that recalculates the magnetic field pattern into the coordinates and orientation angles.

In this project, the Kalmus' guidance method has been successfully implemented for robot navigation. The method, first proposed by Henry Kalmus,[4] was originally designed to aid vehicles

to follow one another. In his method, the two crossed excitation coils are fed from a low frequency source (kHz) in phase quadrature ($\pi/2$ -phase shift). The sensor head placed on a moving platform comprises the two crossed pickup coils and changes its azimuthal orientation with respect to the line of sight between the excitation and sensor heads. It has been shown that the orientation can be determined by measuring the phase difference between the pickup voltages. This principle has been used to build a navigation system that forces the slave mobile platform (“tank”) to follow the leading platform. The leading platform is controlled using remote control and carries the transmission coils (source of quasistatic magnetic field), while the slave platform carries the pickup coils that provide information on the distance from the source of magnetic field and its angle position with respect to the slave platform. Based on a short research, this is the first use of inductive sensors for robot navigation. To adapt the Kalmus’ guidance method, modern electronic components and digital signal processing techniques has been used.

Electric and magnetic fields induce very weak currents in the human body. The purpose of the maximum exposure levels recommended by the ICNIRP, IEEE and ACGIH is to limit these induced currents to levels presenting no health risks.[5] At this time, technology does not allow us to measure currents induced inside the body directly. However, their intensity can be estimated using models of the human body of varying complexity. Another possibility is to calculate induced voltage instead of induced current, as the IEEE has done. Current implementation of the inductive sensor works well below the maximum exposure level, but this issue must be additionally investigated.

The following types of sensors often used for navigation purposes:

- Optical
- Ultrasonic
- GPS
- Wi-Fi (currently in research)
- Accelerometers and Gyroscopes
- Wheel encoders

Optical sensors have variety of approaches, the most simple is the infrared (IR) sensor used to acquire the distance to the objects. Its principle of work is based on emitting infrared light with known intensity and measuring the intensity of the light that comes into receiver that has a filter on it

to cut all other frequencies. Therefore, the lower the intensity, further the object. It can be used for object avoidance and building environment map. The disadvantage of it is a limited range and the fact that the result of reading depends on the surface colour.

A laser range finder uses time of flight (TOF) of the laser instead of intensity that makes it more accurate but also more expensive than IR sensors since precision of sub-nano second ranges requires advanced circuitry. Laser range finder is widely used outdoors due to its accuracy and long distance measuring capability. Issues related with this sensor are high cost, inability to measure transparent objects and sensitivity to bright conditions (direct sunlight).

Another approach is camera based navigation, the most computationally intensive method that requires advanced algorithms to recognise objects, but it also makes it the most configurable approach, as depending on the program, the goal can be changed. Camera problems include complexity of the coding, susceptibility to lightning conditions, requirement of high processing power and line of sight requirement.

Ultrasonic is similar to IR, but uses sound waves instead of light intensity to measure distance. Principle of work is based on sending the sound wave, starting the count and stopping it when the wave comes back. Knowing the approximate speed of sound the distance travelled by the wave is found. Ultrasonic sensors suffer from low accuracy, slow sampling rate and acute angle sensitivity.

GPS can only be used outdoors and provides varying degree of accuracy. Generally used to plot the path, instead of local navigation. It is susceptible to weather conditions and external conditions (city with tall buildings)

Wi-Fi localisation has a number of technologies that could be implemented such as:

- RSSI and lateration based
- FP based
- AOA based
- TOF based

The method has an advantage over other technologies, such as being able to use maps built by community or pre-built for particular case (e.g. office robot) which simplifies navigation. Also, usually no additional hardware will be required, as wireless points cover most of the buildings.

Potential problems can occur if the metal objects or mirrors are added to the environment that will block or weaken the signal. Also, the environment map will change if the transmitter is moved to a different location.

Accelerometers and Gyroscopes are mainly complementary technologies that only aid navigation due to difficulties related to dead reckoning based purely on these sensors alone. Accelerometer suffers from drift over time and inability to distinguish earth gravity from object acceleration. Gyroscope will show zero if the movement stops. By combining them, better results can be achieved, as sensor fusion mostly eliminates their individual disadvantages.

Encoders on the wheels produce a pulse for a fixed number of degrees that the wheel turned. By counting pulses and knowing the angle for each pulse it is possible to access how far the wheel turned and hence, how far the robot moved. In practice, robot will quickly accumulate errors and depending on the error growth rate, become unreliable after certain distance. So this sensor can be used reliably for short distances where the error can be corrected before it grows too large.

By comparing existing sensor applications and their limitations, it can be concluded that the Kalmus' method has one distinct advantage over visual and ultrasonic sensors, which is the fact that no direct line of sight is required. Although the disadvantage here is that both objects that need to be tracked has to be paired. In this context, Wi-Fi technology has a similar set of advantages and disadvantages, although it uses different principles based on electromagnetic waves, not magnetic fields, which allows it to cover larger area. Therefore, for maximum efficiency and flexibility of mobile robot navigation, sensor has to be fused with another sensor. Taking office robot as an example, fusing data from the Kalmus' sensor and laser range finder will provide the robot with ability to navigate the environment and deal with kidnapped robot problem.

3. ADAPTATION OF KALMUS' GUIDANCE METHOD FOR SPECIFIC APPLICATION

Originally, the method was designed to aid vehicles to follow one another. Two measurements have to be performed in the tracking vehicle B : the distance to the leading vehicle A has to be measured; and the angle between the direction of motion of B (its horizontal axis) and its line of sight to A must be determined. This information is sufficient to steer B in such a way that it is always following A , maintaining a certain distance. The system can be used either for fully automatic steering of vehicles, or as an aid for the driver in the conditions of poor visibility (night, smoke, fog or cloudiness). In robotics, Kalmus' method could be used to guide a mobile robot or a group of mobile robots.

3.1 Kalmus' guidance algorithm

A scheme of the Kalmus' guidance method adapted for this application using modern components is shown in Fig. 1. Two crossed excitation coils (ensuring minimum mutual inductance) are fed from a quadrature generator, i.e. the first coil has the excitation voltage $A \cos(\omega t)$ and the second coil – $A \sin(\omega t)$. The excitation amplitudes and frequencies (kHz range) are the same for both coils. At sufficiently far distance (much larger than the characteristic dimension of coils), these coils create a rotating magnetic field in each point on the horizontal plane. According to Faraday's law, [1] an electromotive force (e.m.f.) $V_{out}(t)$ will be induced in a pickup coil placed in any point of the horizontal plane and having the cross section perpendicular to this plane:

$$V_{out}(t) \sim N \frac{d\Phi(t)}{dt} \quad (1)$$

where $\Phi(t)$ is the alternating magnetic flux through the pickup coil, caused by the rotating magnetic field, and N is the number of coil turns.

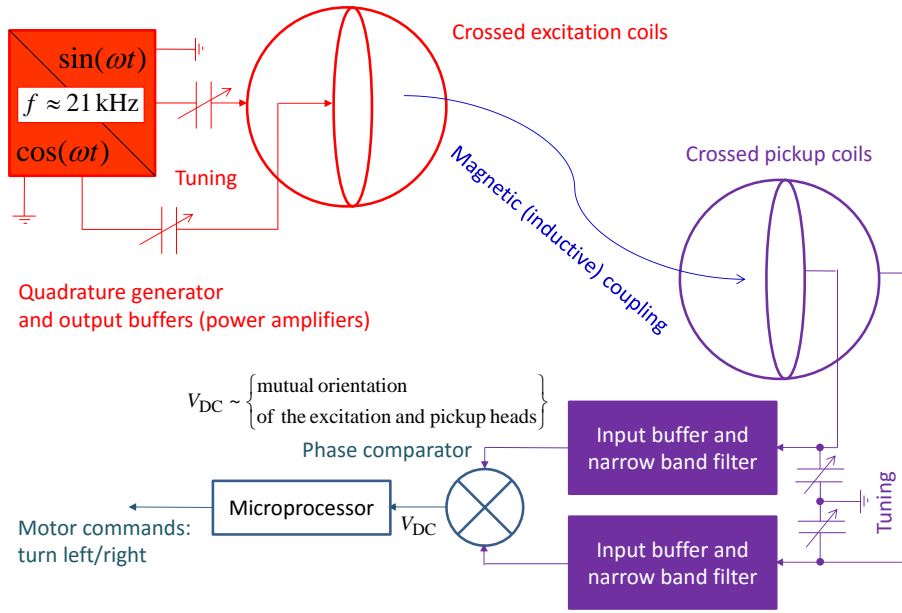


Fig. 1. Kalmus' guidance method adapted for this application using modern components.

If there is a system of two crossed pickup coils (again to minimise their mutual inductance), two e.m.fs. $V_{out}^1(t)$ and $V_{out}^2(t)$ shifted by phase will be induced in them. As it has been shown in Ref. [4], this phase difference $\Delta\eta$ depends on the in-plane orientation of the assembly of crossed pickup coils with respect to the excitation head (see Fig. 2) also consisting of two crossed coils:

$$\Delta\eta = \tan^{-1}\left(\frac{4}{3\sin(2(\psi - \varphi_0))}\right) \quad (2)$$

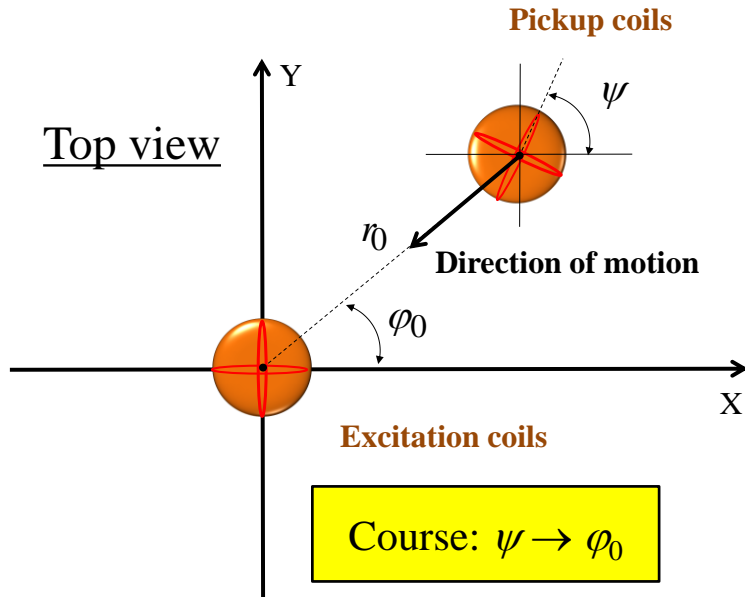


Fig. 2. The orientation scheme used in Kalmus' method.

The arctangent function in Eq. (2) will be understood as the function ATAN 2(y, x):[6]

$$\text{ATAN 2}(y, x) = \begin{cases} \tan^{-1}\left(\frac{y}{x}\right), & x > 0 \\ \tan^{-1}\left(\frac{y}{x}\right) + \pi, & y \geq 0, x < 0 \\ \tan^{-1}\left(\frac{y}{x}\right) - \pi, & y < 0, x < 0 \\ +\frac{\pi}{2}, & y > 0, x = 0 \\ -\frac{\pi}{2}, & y < 0, x = 0 \\ \text{undefined,} & y = 0, x = 0 \end{cases} \quad (3)$$

$$\Delta\eta = \text{ATAN 2}(4, 3\sin(2(\psi - \varphi_0))) \quad (4)$$

The graph of $\Delta\eta(\alpha) = \text{ATAN 2}(4, 3\sin(2\alpha))$, where $\alpha = (\psi - \varphi_0)$, is shown in Fig. 3.

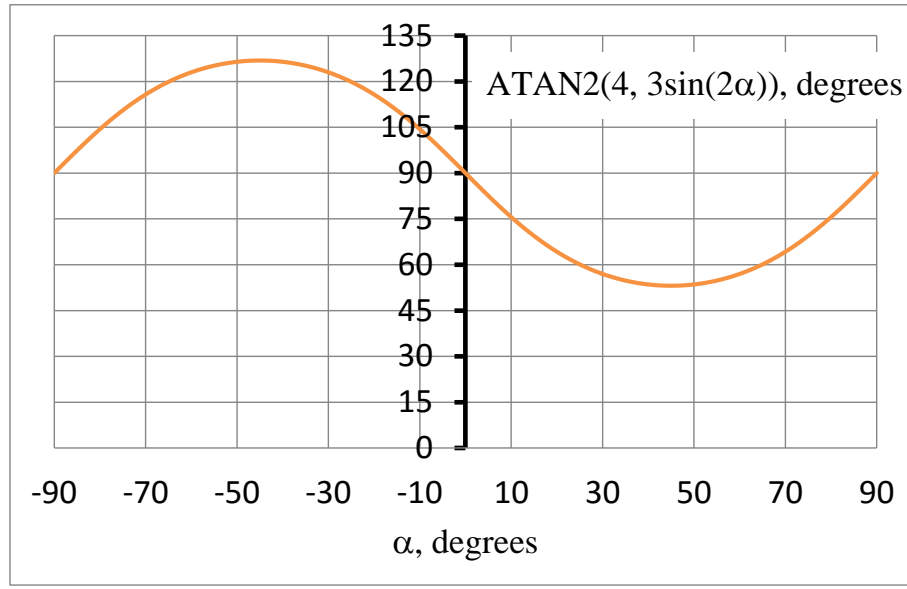


Fig. 3. The graph of $\Delta\eta(\alpha) = \text{ATAN } 2(4, 3\sin(2\alpha))$ for $\alpha \in [-90^0, 90^0]$.

Non-ambiguous direction indication can be obtained as long as $|\alpha|$ does not exceed 90^0 :

$$\begin{cases} -90^0 < \alpha < 0 \Rightarrow 90^0 < \Delta\eta(\alpha) < 126.87^0 \\ 0 < \alpha < 90^0 \Rightarrow 53.13^0 < \Delta\eta(\alpha) < 90^0 \end{cases} \quad (5)$$

Finally, we obtain a very simple guidance algorithm when moving to the centre where the excitation head is placed:

Turn right, if $\Delta\eta < 90^0$
or
Turn left, if $\Delta\eta > 90^0$

The amplitudes $|V_{out}^{1,2}(t)| \sim \frac{1}{r_0^3}$ and can be used to measure the distance (after a calibration).

3.2 Design strategy of excitation coils

The quadrature generator providing the excitation sinusoids in a circuit is a low power chip. To allow a larger current through the coils, the sinusoids were passed through the buffers playing the role of power amplifiers. However, this is not enough because the impedance of excitation coils contains a large inductive part at the excitation frequency $f \approx 21$ kHz:

$$Z_{excit} = R + i\omega L \quad (7)$$

where R is the coil DC resistance, $\omega = 2\pi f$ is the angular frequency, L is the coil inductance, and $i = \sqrt{-1}$ is the imaginary unit. The inductive part in Eq. (7) can be compensated by a tuning capacitance C connected in series with the coil as shown in Fig. 1 (red). In this case, the total impedance is:

$$Z_{excit} = R + i\omega L - \frac{i}{C\omega} = R + i \left(\frac{\omega^2 LC - 1}{C\omega} \right) \quad (8)$$

Choosing C from the condition:

$$C = \frac{1}{\omega^2 L} \quad (9)$$

the total impedance Z_{excit} in Eq. (8) becomes purely real. This is the current resonance condition.

For winding the excitation coils, AWG-34 (diameter 160 microns) copper wire was chosen [7] to allow the DC current of 56 mA (or AC current of 79 mA). The maximum output current of the buffer chip was 70 mA (DC). With the AC excitation amplitude 10 V and $R = 143 \Omega$, we obtain a let-go current 70 mA (AC amplitude). The excitation coils were wound to have $R \sim 143 \Omega$. This condition resulted in a certain inductance L (determined by the coil geometry), which can be measured by an inductance meter. Then, the required value of C was found using Eq. (9). So, it was the decision in the design strategy that guaranteed a safe large current through the excitation coils. At the conditions $\text{Re}[Z_{excit}] \equiv R$ and $\text{Im}[Z_{excit}] \equiv 0$, the excitation current and voltage will be in phase (current resonance).

3.3 Design strategy of pickup coils

The pickup coil circuits were also tuned to obtain the maximum voltage outputs before entering the buffers and narrow band filters (violet in Fig. 1). The equivalent circuit of a pickup coil is shown in Fig. 4. We are interested in maximising the voltage amplitude measured across the tuning capacitance C , which is now connected in parallel to the pickup coil:

$$V_C = V_{out} \times \frac{i\omega C_p (R + i\omega L) + 1}{i\omega R(C + C_p) + 1 - \omega^2 L(C + C_p)} \quad (10)$$

where

$$G(\omega) = \frac{i\omega C_p (R + i\omega L) + 1}{i\omega R(C + C_p) + 1 - \omega^2 L(C + C_p)} \quad (11)$$

is the pickup coil transfer function from the externally induced voltage $V_{out} \sim \exp(i\omega t)$ to the capacitance voltage $V_C(t)$. This transfer function changes the phase and amplitude of a harmonic $V_{out}(t)$. The voltage resonance condition will be achieved for the following frequency:

$$f_{res} = \frac{1}{2\pi\sqrt{L(C + C_p)}} \quad (12)$$

At $f = f_{res}$, we obtain:

$$G(\omega)|_{\omega=2\pi f_{res}} = \frac{iC_p(\sqrt{L(C + C_p)}R + iL) + L(C + C_p)}{iR\sqrt{L(C + C_p)}(C + C_p)} \quad (13)$$

Neglecting the parasitic shunting capacitance C_p , we obtain:

$$G(\omega)|_{\omega=2\pi f_{res}} \approx -iQ \quad (14)$$

where

$$Q = \frac{1}{R} \sqrt{\frac{L}{C}} \quad (15)$$

is called the coil quality or Q-factor.[8] Q-factor works as a coil amplification (voltage resonance). To maximise this coefficient, we have to increase the coil inductance, while keeping its resistance as small as possible. That can be achieved by using a ferrite core and reducing the number of coil turns. The wire diameter is not a critical parameter because the induced currents are very weak. So, it was specifically designed design strategy that guaranteed the maximum voltage outputs from the pickup coils.

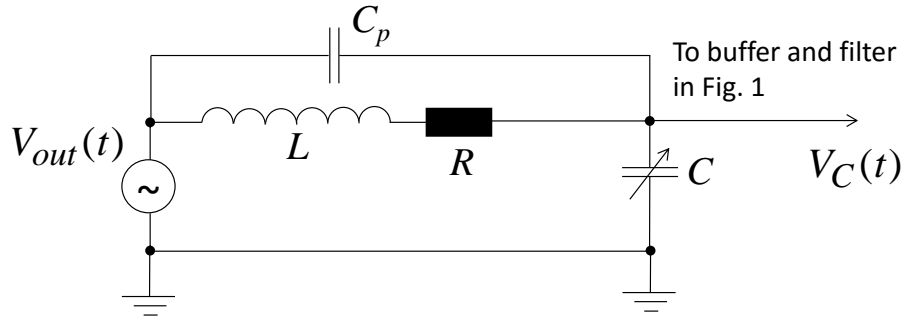


Fig. 4. Equivalent circuit of a pickup coil, where $V_{out}(t)$ is e.m.f. induced by the external alternating magnetic flux as explained in Eq. (1), C_p is a parasitic shunting capacitance, and C is a tuning capacitance used to obtain the voltage resonance condition for $V_C(t)$.

Let us note that the optimisation of the excitation and pickup circuits using their resonance tuning is similar to that used in the non-radiative wireless power transfer technology.[9] “Non-radiative” because we use quasistatic excitation and inductive coupling between the excitation and pickup coils (transformer principle).

Now, the main advantages and disadvantages of the proposed sensor method can be listed:

Advantages

- Transparency to non-metallic objects
- Cheaper than optical systems
- Not prone to external conditions such as brightness, smoke etc.
- Real-time feedback is available

- Multiple systems can work in the same environment while using different frequencies

Disadvantages

- Electrical and magnetic noise may affect the readings
- Metal objects in close proximity may result in a distortion of the pickup voltages
- Configuration is difficult to change
- Frequencies that can be used has to be much smaller than system size to avoid electrical interference
- Lower sampling rate

4. PROJECT STAGES

The project aim is to develop the sensor system capable of using low frequency magnetic field to receive heading and distance information about the transmitter. Based on this requirement, the project was divided into the following stages:

1. Developing coil design small enough to fit on mobile platform but powerful enough to be able to create omnidirectional magnetic field for a maximum distance up to several meters (taking into account noise).
2. Developing quadrature oscillator source for the transmitter.
3. Developing filter that is essential for sustaining correct information about the phase of pickup voltages.
4. Developing phase detection circuit or algorithm to guide the receiver platform to the transmitter.
5. Control system to analyse the phase of pickup voltages and based on it control the platform's motors to follow the transmitter.

To provide additional layer of security against failure, a modular design has been used. For this, all circuit boards carry out just one task but can be fed from one source. In this scenario, if one board fails or there is a critical mistake in the design that led to component damage, it is limited to one PCB and the cost to replace the board and components is less. The following implementation plan was used:

- First, physical properties of the system have to be taken into account to optimise signal transfer from the transmitter to the receiver. Since the principle of inductive coupling is used, the coils must be tuned to enhance the response (recall the current and voltage resonances discussed in Section 3). Wire gauge, current, voltage, and size of the coil has to be determined.
- Second step will be done using quadrature oscillator based on a single chip that will provide the excitation sinusoids for operational amplifiers configured as the voltage followers (buffers) to boost current output of the oscillator chip.

- Third step is developing narrow band filters to suppress noise and boost the useful signals induced in the pickup coils. To achieve the best results, a filter design utility from Linear Technology will be used.[10]
- Phase detection circuit will include a comparator configured as the null detector. Additionally, if the comparator fails, an external analog phase detector circuit can be used. Actual phase difference will be determined using microprocessor or FPGA.
- FPGA or microprocessor will analyse the signals induced in the pickup coils using either the voltage given by the phase analysing module or the time between edges of the square waves after the comparator. The phase will be determined providing information on the direction of the receiver according to the algorithm (6). Then, FPGA will generate commands for the motor drivers.

5. BUSINESS CASE RESEARCH

Potential market for the modern implementation of the Kalmus' algorithm involves industrial use and research purposes. For industrial use, potential applications may involve navigation in the storage environment of the robots, usage for creating a car trains on highways or in traffic jams, or navigating the robot hand.

Total cost of the project calculated in the Table below can potentially be decreased by using more specialised components, e.g. non-configurable filters, buying components in bulk and ordering PCBs in bulk, and using specialised circuits for the phase and amplitude detection and motor drivers instead of FPGA.

Power and input circuit	£21.54
Filter circuit	£49.108
Transmitter circuit/platform	£31.286
Comparator circuit	£26.259
Controller board	£75.15
Additional components	£128.786
Unused components	£0.96
Total cost	£332.129

Additional components were the biggest cost factor. This category involves connectors, platforms, and jumper wires. Filter circuit involves universal filters and high precision resistors, therefore, costing more than standard filtering circuit. Comparator circuit cost could be decreased if no backup circuit and slower comparator circuit would have implemented. In the project, some of the components have not been used but their cost has been accounted for as well. Full description of all components that has been used can be found in [10.4 APPENDIX 4: Project materials and cost full graph.](#)

6. DESIGN SPECIFICATION

This section contains all specifications regarding the production moments, circuit schematics and specific components that has been used on the project. Full sized diagrams are available in the [10. 2 APPENDIX 2: Full sized circuit diagrams](#)

6.1 Fabrication of the excitation and pickup coils

The excitation coils were wound on wooden cylindrical cores, shown in Fig. 5, according to the design strategy described in Section 3.2. They required a significant number of turns that would be difficult to count during the fabrication process. To simplify the task, first the full length of wire ~ 164 m, which provides the resistance $\sim 143 \Omega$ required by the design, was unwound from the bobbin on a wood frame. Then, this length was rewound turn to turn on the coil wooden core. The coils characteristics are given in the table below:

Parameter	Value
Total length of the wooden core, including flanges	103 mm
Wooden core diameter	18 mm
Wire diameter	0.16 mm (AWG-34)
Effective coil length	93 mm
Total number of layers	6
Factual coil resistance	$\sim 144.5 \Omega$

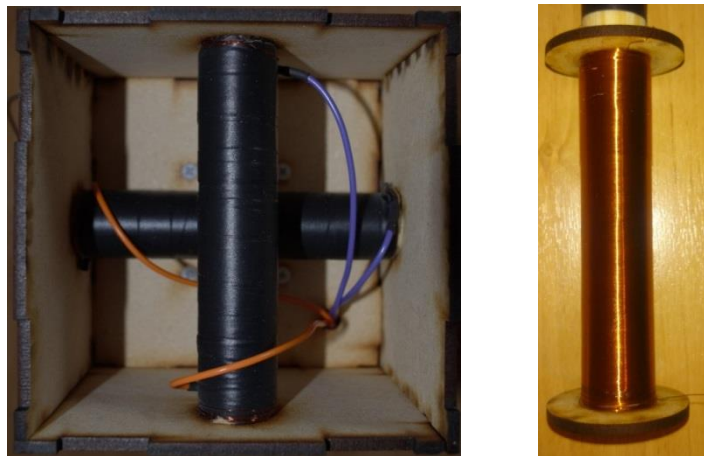


Fig. 5. Excitation coils: wooden frame with flanges and final assembly in the box. The crossed coils have a minimal mutual inductance and cross talk.

The pickup coils were wound on ferrite cylindrical cores, shown in Fig. 6, according to the design strategy described in Section 3.3.

Parameter	Value
Total ferrite length	100 mm
Ferrite diameter	9.5 mm
Wire diameter	0.1 mm
Effective coil length (excluding the flanges)	87 mm
Total number of layers	2
Coil resistance	$\sim 95.5 \Omega$

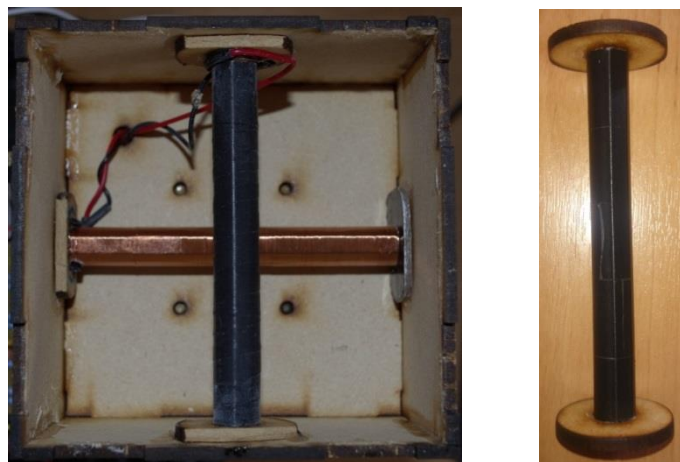


Fig. 6. Pickup coils: ferrite frame with wooden flanges and final assembly in the box. The crossed coils have a minimal mutual inductance and cross talk.

To make the boxes for transmitter and receiver, poles for them and end caps for coils themselves SolidWorks software has been used. Detailed mechanical drawings are available in [APPENDIX 1: Mechanical drawings for components](#)

6.2 Design of the transmitter electronic circuit

Excitation circuit creates the magnetic field using a set of two coils supplied with power from operational amplifier. Op-amp is driven from quadrature oscillator that creates two waveforms with 90 degrees phase shift. Fig. 7 shows main components of the circuit and short description of each is given below:

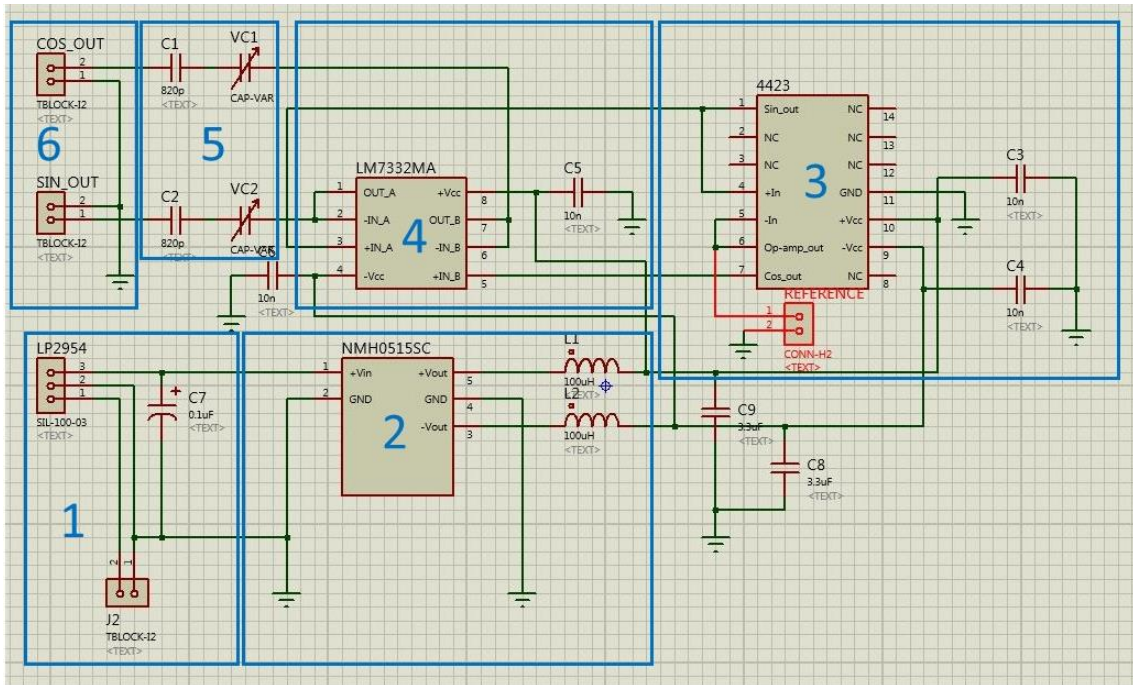


Fig. 7. Excitation circuit schematic.

1. Battery is connected to the screw-in terminal, which in turn connected to the LP2954 voltage regulator that outputs 5 V. This component has been chosen specifically due to its low dropout voltage, meaning that it will be able to work longer on batteries. To suppress the ripple on the output of the voltage regulator, 0.1uF decoupling capacitor is placed on the power line.
2. Murata NMH0515SC acts as a dual rail booster, increasing the voltage from the LP2954 to +15 and -15 Volts. It has been chosen for the fact that all the necessary components are built into the case, meaning that only ripple filtering stage is required. On the output of the chip, inductor of value 100uH and decoupling capacitor are placed, following the recommendations given in the datasheet for the component. This setup will filter out the ripples from the NMH0515SC and help obtain stable DC voltage. The maximum power that

this component is able to supply is 2 W, so this limits the maximum power that can be transmitted as well as affecting the choice of the operational amplifier.

3. Quadrature oscillator 4423 is used to create two phase shifted waveforms with the maximum amplitude of 10 V. Chosen for its compactness, low power requirements, and sufficiently stable output. Supply voltage is +15 and -15 Volts given by Murata chip, also, to increase the stability of the output, two decoupling capacitors of 10 nF are placed close to the power supply inputs of the chip. The outputs of the chip has to be boosted in terms of current, which is achieved in the Section 4, using the operational amplifier.

Additionally, to simplify the testing further on, one of the inputs of the chip is fed through built in operational amplifier so that the waveform can be sampled using oscilloscope and checked for stability and integrity.

4. Operational amplifier LM7332MA is configured as a current boosted, providing a maximum of 70 mA per channel, while also electrically insulating the quadrature oscillator from the coils. The chip has a low internal current requirements and provides sufficient current output for the purpose. The supply used for this component is also +15 and -15 Volts and to provide stable power supply to the components, 10nF capacitor is used for decoupling.
5. Tuning stage consists of fixed value and variable capacitor. The outputs from operational amplifier are fed into capacitor connected to the coil in series, effectively making the LC series circuit that allows to tune the coils to achieve maximum power transmission. Variable capacitor allowed to make fine tuning to the value of the fixed capacitor, however, this type of capacitor is susceptible to the changes in temperature. To minimise the effect of the temperature on a capacitors, high quality ceramic capacitors has been used, with a precision in the range of $\pm 10\%$.
6. Output stage, capacitor outputs are connected to the coils through screw-in terminals that allowed to quick changes during the testing. Second pin of the screw-in terminal is grounded.

The resultant circuit is shown in Fig. 8.

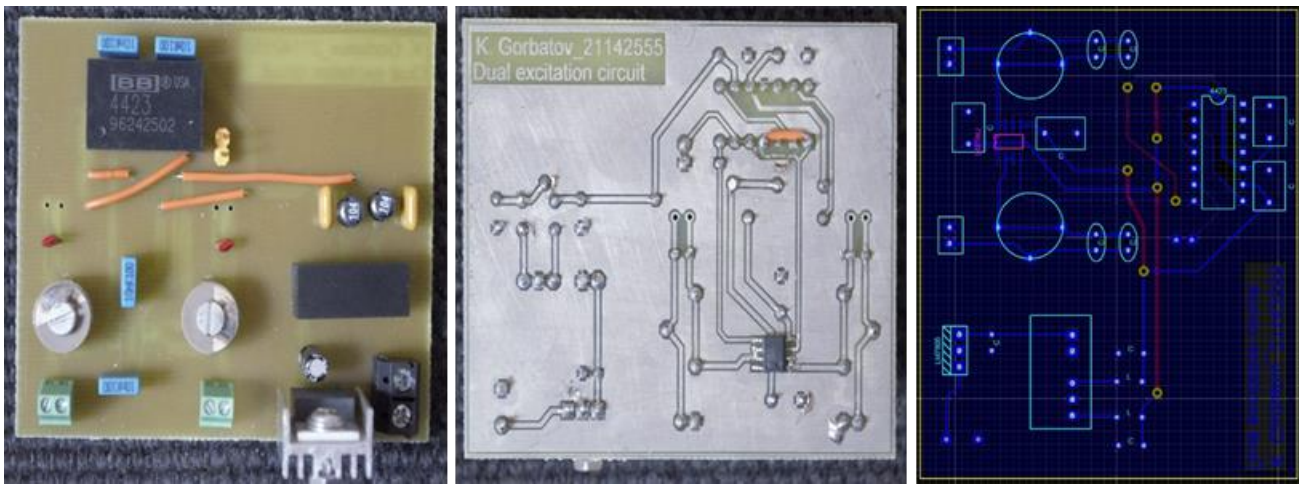


Fig. 8. Fully assembled excitation circuit.

6.3 Design of the Power and Tuning stage circuit

This circuit receives the signal from the coils, allows to tune the coils using tuning stage, passes the signal through the operational amplifier to separate coils from the rest of the system and supplies filter and comparator circuits with power. Fig. 9 shows all components of the circuit and each component is described shortly below.

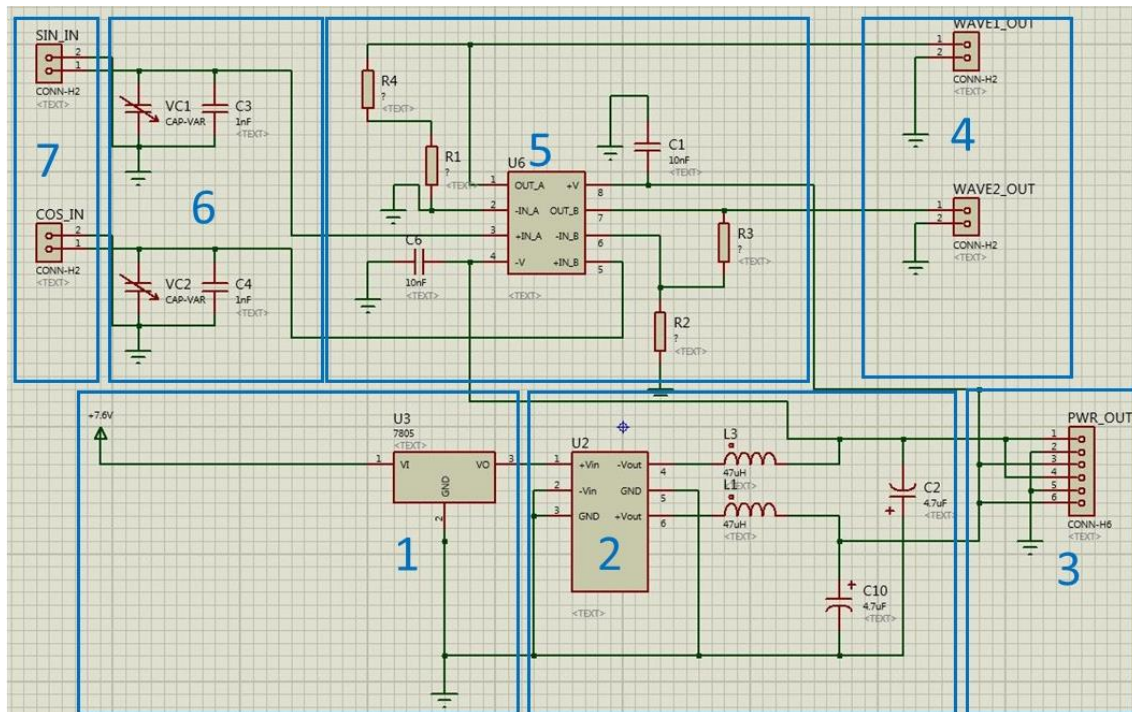


Fig. 9. Input and Power circuit schematic.

1. LP2954 does the same role here as in excitation circuit, voltage regulator is fed from the battery connected to the screw-in terminal and the output of the chip is 5 V. This component has been chosen specifically due to its low dropout voltage, meaning that it will be able to work longer on batteries. To suppress the ripple on the output of the voltage regulator, 0.1uF decoupling capacitor is placed on the power line.
2. Murata NMH0505SC acts as a dual rail voltage splitter, creating from single 5 V source +5 and –5 Volts. It has been chosen for the fact that all the necessary components are built into the case, meaning that only ripple filtering stage is required. On the output of the chip, inductor of value 47 uH and decoupling capacitor of 4.7 uF are placed, following the recommendations given in the datasheet for the component. This setup will filter out the ripples from the NMH0515SC and help obtain stable DC voltage. The maximum power that this component is able to supply is 2 W.
3. 6 terminal headers are used to supply comparator and filter circuit with power
4. Output from the operational amplifier (5), goes into filter circuit. Two terminal headers are used for each channel and to protect the signal from electromagnetic interference, the wires have been intervened.
5. Operational amplifier LM7332MA, in this case configured as a voltage follower. However, to account for the possibility that the signal from the coils will be too low, additional holes has been made so that gain can be increased using resistors. Initially, these holes were connected with wires, so that the gain is 1 and the signal goes unchanged into filter. Supply voltage is +5 and –5 Volts, therefore limiting the input voltage. Decoupling capacitors are same as with the excitation circuit, 10 nF.
6. Tuning stage, capacitors has been placed in parallel, making it a parallel LC circuit. For temperature stability and better precision ceramic type of fixed capacitor of 1330 pF has been used. Variable capacitor is the same type that has been used in excitation circuit – 8 pF to 50 pF.
7. Screw-in terminals connecting the coils to the capacitors

The resultant circuit is shown in Fig. 10.

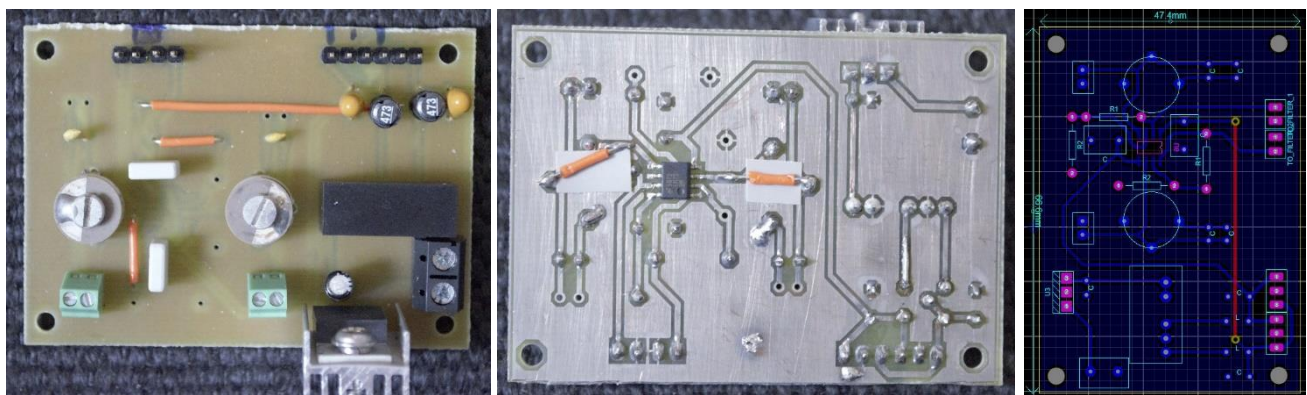


Fig. 10. Fully assembled Tuning and Power circuit.

6.4 Design of the filter circuit

To speed up the development and ensure best results, filter design has been generated in Linear Technology utility [10] that allows to fine-tune required bandpass area and other properties. The required properties of the filter is a sharp cut-off after central bandpass frequency and high noise rejection. To provide sharp cut-off Chebyshev type of filter has been used as it is known for steep roll-off, although at the cost of passband ripple, however, design utility has been configured to move the ripple into stopband region. Whilst, providing smooth response in passband as shown in Fig. 11 below.

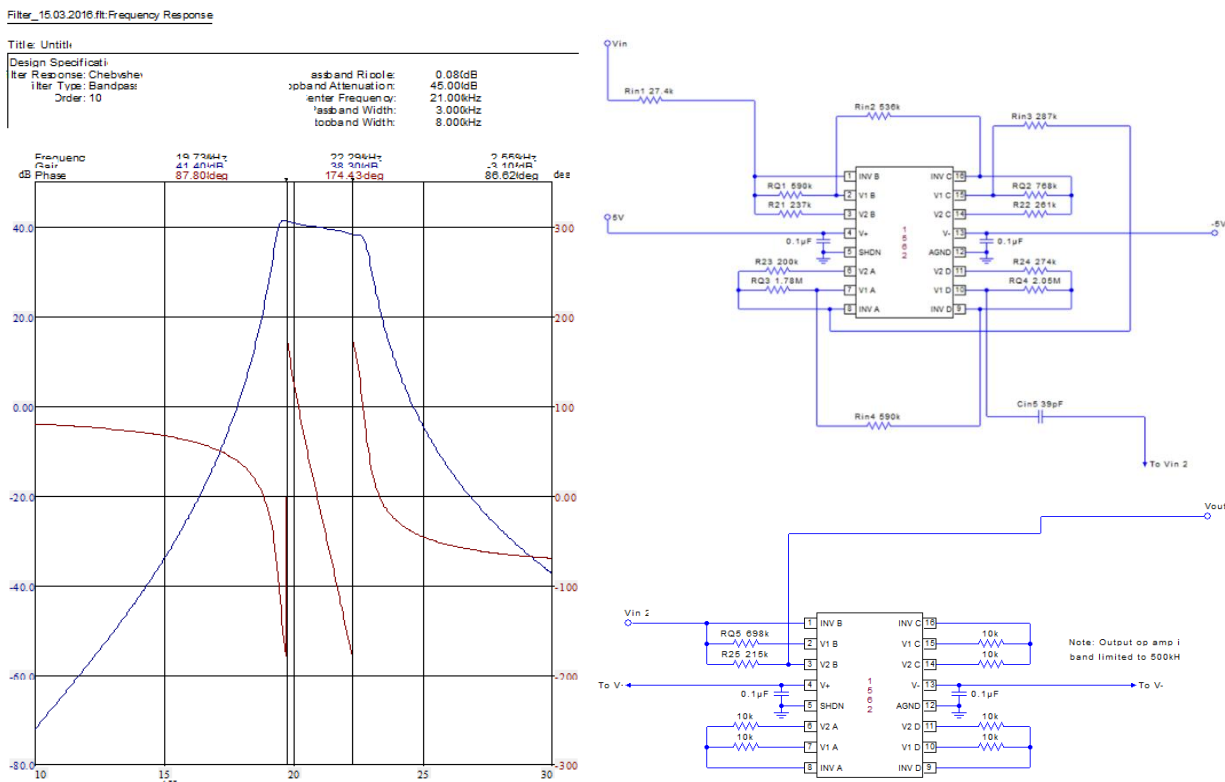


Fig. 11. Predicted passband response of the filter (left) and generated schematic of the filter (right).

The circuit that is generated by the utility uses LTC1562 chip, which is the configurable filtering block that works in the centre frequencies of 10 kHz to 150 kHz. Therefore, to achieve stated properties, two chips are required for each signal, meaning four chips in total has been used.

Schematic from Proteus is shown in Fig. 12.

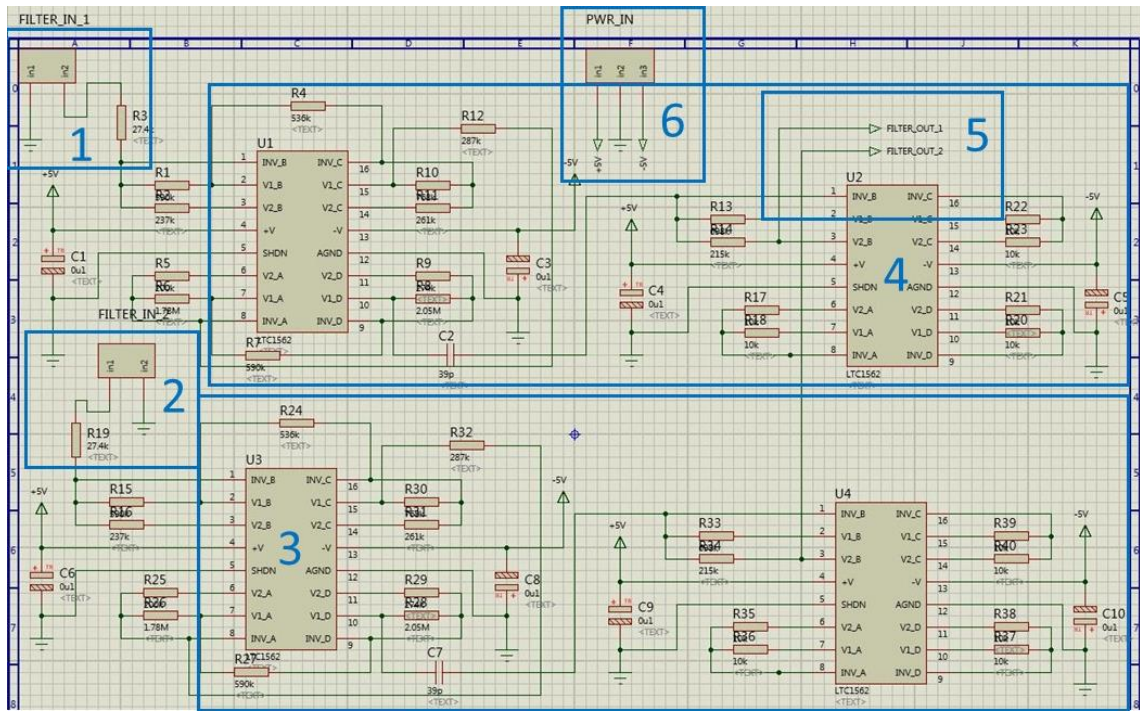


Fig. 12. Filter schematic from Proteus software.

1. Channel 1 input into filter 1, wire has been twisted to ensure some electromagnetic protection.
2. Channel 2 input into filter 2, wire has been twisted to ensure some electromagnetic protection.
3. Filter 2 circuit, consisting of two LTC1562 connected one after another but with different resistors.
4. Filter 1 circuit, identical to filter 2. Consists of two LTC1562 connected one after another but with different resistors.
5. Filter outputs, in the physical circuit taken in the middle between two filters to ensure fair noise distribution.
6. Power coming into the filter ±5 Volts.

Resultant circuit is shown in Fig. 13 below.

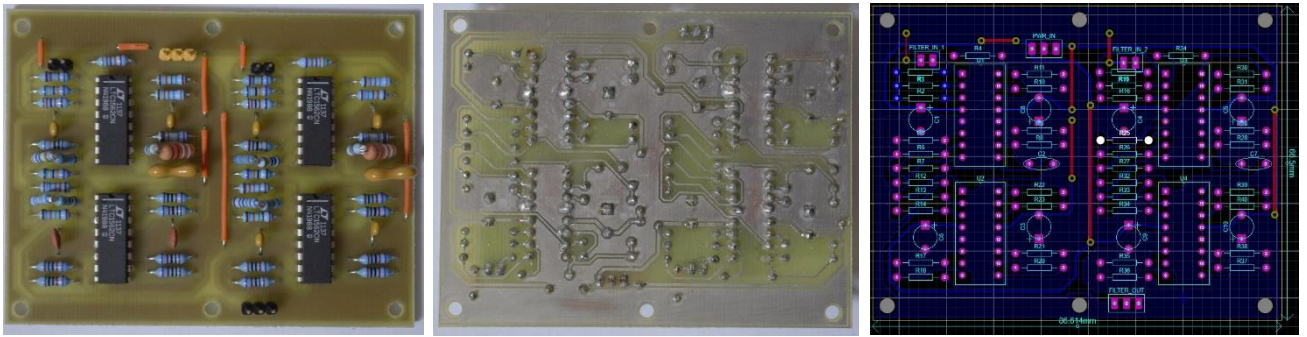


Fig. 13. Filter circuit fully assembled.

During assembly, resistors with 1% of variation has been used to ensure that the frequency response of the device will be the same as planned. Effort has been put to ensure that traces from input and output are kept as short as possible from their destinations until the input or output pins. Also, both filters have almost exact same configurations on PCB to ensure that both signals will be subjected to the same noise or voltage drops. Input and output cables has been twisted to cancel out electromagnetic interference. Initially it has been planned to cover the twisted cables in copper tape shielded to the ground for extra layer of protection, but after testing it became evident that this measure is excessive and restricts the movement of the cable and poses the risk of shorting for nearby circuits.

6.5 Design of the comparator circuit

Comparator circuit receives two inputs from the filter and creates a square wave from them using the method called null detection. So that when wave goes into positive cycle, from negative and crosses 0, rising edge is created on the output of the comparator, same applies to the positive to negative cycle, but this time falling edge is on the output and 0 V is kept until wave will go into positive cycle again. Main components of the circuit are given in Fig. 14 as well as short description of each component below it.

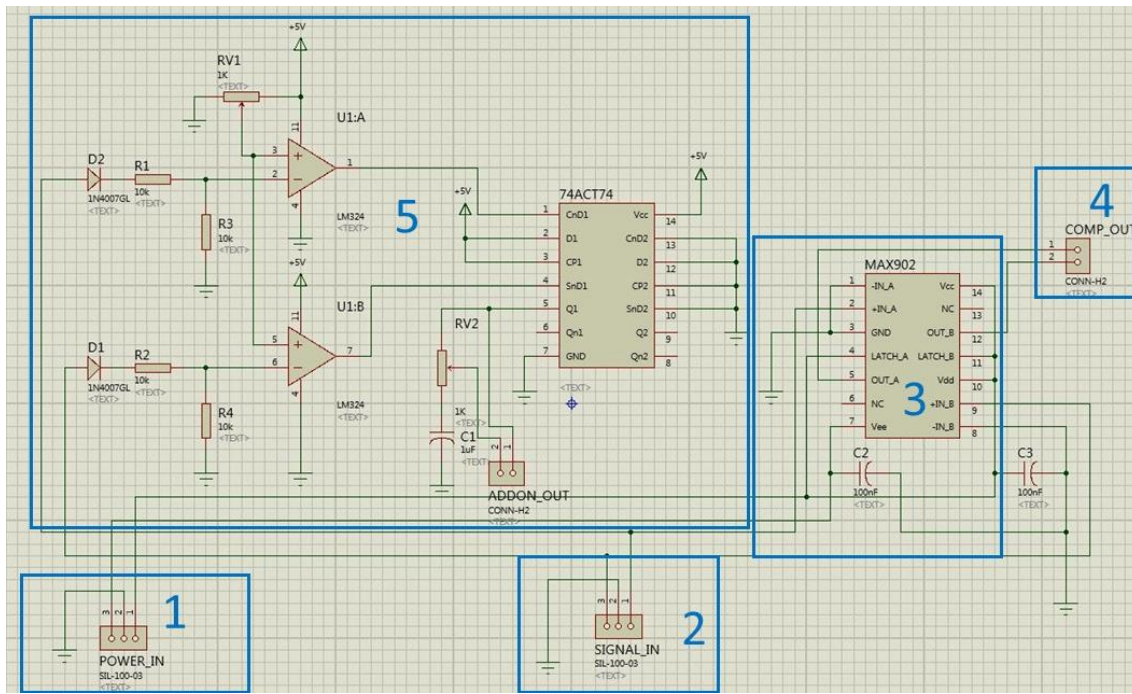


Fig. 14. Comparator circuit schematic.

1. Power supply to the circuit, ± 5 V with the ground in the middle.
2. Two channels input with the ground in the middle for reduced electromagnetic interference.
3. MAX902 comparator receives the signal from two channels and processes them independently. Square wave is created at any point when signal goes from positive to negative cycle (0 V on the output) or from negative to positive (5 V on the output). This particular comparator has been chosen for its high response speed and ability to output configurable voltage (set by Vdd). In this case Vdd has been connected to the positive supply rail as 3.3 V used by FPGA are beyond the limit of component. Power supply to the component are standard ± 5 V with decoupling capacitors 100nF, as advised in the manual.
4. Output of the comparator, goes to logic level shifter that will convert 5 V to 3.3 V which is an acceptable range of the FPGA.
5. Backup circuit designed from cheap parts to ensure that if comparator performance will be insufficient it can be used instead. It consists of two main parts – LM324 amplifier and 74ACT74 Dual D-Type Positive Edge-Triggered Flip-Flop. Amplifier allows signals only within certain range, set by variable resistor. Flip flow produces the signal whenever there is an area where two signals are in phase. The length of the signal correspond to the phase of two signals.

However, since comparator worked well, the backup circuit has been physically disconnected from the rest of the circuit so that it does not consume any extra power.

The resultant circuit is shown in Fig. 15.

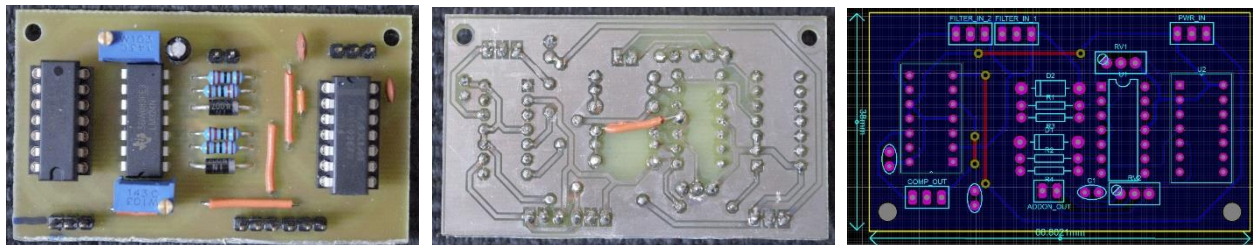


Fig. 15. Comparator circuit fully assembled.

6.6. Controller circuit

Controller system consists of two main parts: hardware and software. Hardware part consists of logic level shifters, LEDs, power supply and motor controller. Software part contains the actual control of the motors, LEDs and phase determination logic.

6.6.1 Hardware specification

During the initial project phase, a number of different approaches have been analysed. They are listed below:

- Analog based phase detection system where phase is given out in the form of analog signal proportional to the phase. Microcontroller unit would only need a relatively slow ADC (Analog-to-Digital converter) to sample phase periodically and control the motors.
- Purely digital system where fast ADC would sample both signals either at the same time or in turn and calculate phase using microcontroller that would control motors appropriately.
- Mixed system where signal is fed into either a comparator or similar device to get a finite number of pulses per wave, those pulses would be analysed by microcontroller, phase calculated and depending on which, motors controlled.

Each approach has a number advantages and disadvantages and varies in complexity. First method is the fastest and requires little programming as the speed of sampling the phase is slow and fast response is not required as platform will change its position slow enough relative to signal

frequencies. Suitable microcontroller that has been considered were STM Discovery and Arduino. However, due to the fact that all of the circuits considered were able to detect only phase, without providing data on sign of the phase, additional comparator circuit the idea has been abandoned.

Second approach was considered next, the system without analog parts and based purely on microcontroller unit. This method is simple in terms of circuit design, but difficult in programming part as it would require sampling at least twice as fast, according to Nyquist theorem. Two systems that have been considered for this task were STM Discovery and DEO-NANO FPGA, first being typical microcontroller system with built-in ADC and second being field programmable gate array that has an ability to process data fast enough and also carries on-board ADC. Test programs has been written for both systems and while STM Discovery would be the most suitable controller for this task, the difficulty of using advanced functions such as direct memory access (DMA) and lack of manufacturer support on standard libraries proven to be too time consuming. DEO-NANO on the other hand has been easy to program, but built-in ADC has been too slow to capture transition times accurate enough to use it for measuring time between two signals.

Last approach includes all the positive sides of the aforementioned two methods while having the opportunity for backup plan. Mix of two systems involves using comparator configured as a null-detector to output pulse each time wave goes through zero, this has an advantage of being unsusceptible to the level of the signal as however small the signal is, it's still a wave, which has a transitions through zero. Therefore, microcontroller, or in this case FPGA, will receive purely digital signal that is easy to obtain and measure time between two successive edges. Backup plan mentioned in the beginning, involves leaving extra pins on a PCB board to connect to filter output or external phase analyser, in case signals will be too noisy to analyse them digitally.

So, after considering the factors mentioned above, the decision was to choose the mixed approach and have analog and digital parts in the system. Two main parts of the system are *peripheral board* containing motor controller, power supply, LEDs , logic level converters and 26 pin terminal for DEO-NANO. Another part of the system is DEO-NANO, this FPGA is the most affordable among its competitors which is vital for the project while also containing various peripherals such as ADC, accelerometer and GPIOs. Also, due to the fact that the maximum speed of FPGA is 50MHz, is leaves plenty of room for calculations and filtering of the signals.

Peripheral board receives incoming signal from varying sources, such as:

- Comparator
- Motor encoders
- Infrared sensor

Comparator signals are two square waves with varying phase to each other. These signals are fed through 5 V to 3.3 V voltage regulator so that the amplitude is within acceptable range of DEO-NANO. To acquire the phase difference between signals, edge of the first signal is checked and counter starts, when second wave's edge occurs, counter stops and since frequency has only slight deviations – counter value is known for each phase value. Depending on which wave is leading, directional flags are set, so that the tank can go to the left or right with rotation corresponding to phase amplitude.

In Fig. 16, main parts of the controller circuit are highlighted and short explanation of each component is given below it.

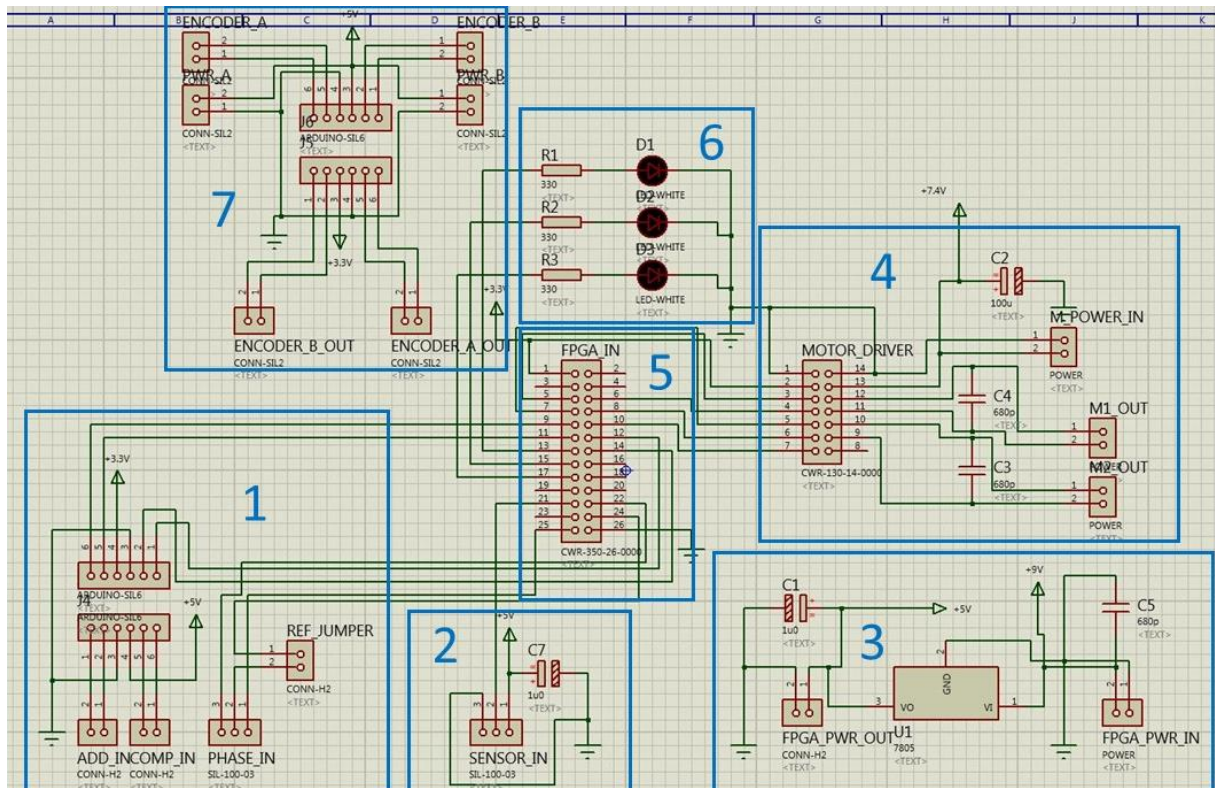


Fig. 16. Controller circuit schematic.

1. Logic shifter part and phase input, logic shifter part is used to convert output from comparator to 3.3 V. Logic shifter is the generic pre-assembled boards based on BSS138 which is the field effect transistor. Chosen for their low price and the fact that they come pre-assembled which saves time. When tested, it has shown that the chip smoothed out edges of the square pulse, but this effect did not affect the performance.
Phase input has been planned to be used to receive output from external phase detector module but have not been used in the end.
2. Analog input from infrared sensor with capacitor on power supply line to ensure that sensor receives enough power.
3. Power supply part of the circuit, LP2954 voltage regulator is used. Input to the component comes from the battery and the output is 5 V. To reduce the output ripple, capacitor has been placed on the output.
4. DRV8835 Dual Motor Driver receives 2 PWM signals and 2 Enable signals for 2 motors. This module allows the maximum of 1.2 A for both motors and has a built-in thermal protection, which means that when it overheats the tank will simply stop until the motor driver cools down. However, the experiments have shown that when loaded with 1kg the tank consumed 550 mA for each motor. The useful load of the tank is estimated to be around 800 g, so the tank will be able to drive for significant amount of time before the motor driver will need to cool down. As a backup option, the heatsink can be attached to the top of the chip, which will significantly increase the thermal limit of the chip.
5. 26 pin header for DEO-NANO
6. 3 on-board LED's are used to demonstrate left, right and straight directions for clarity and easier debugging. Resistors that has been chosen provide 10 mA current using $330\ \Omega$ resistors.
7. Another logic level shifter, used for converting signals from 5 V encoders to standard FPGA voltage of 3.3 V.

Resultant circuit is shown in Fig. 17 below.

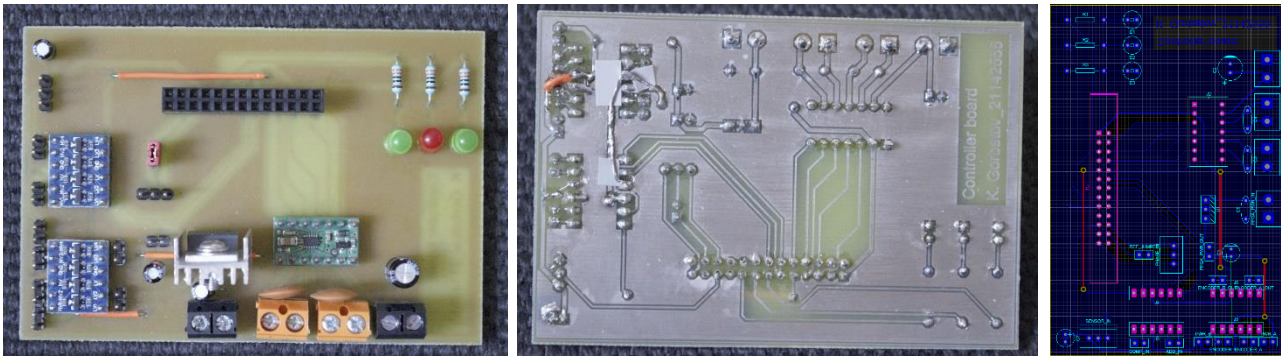


Fig. 17. Controller circuit fully assembled.

6.6.2 Software design

Main design file of the controller is shown in Fig. 18.

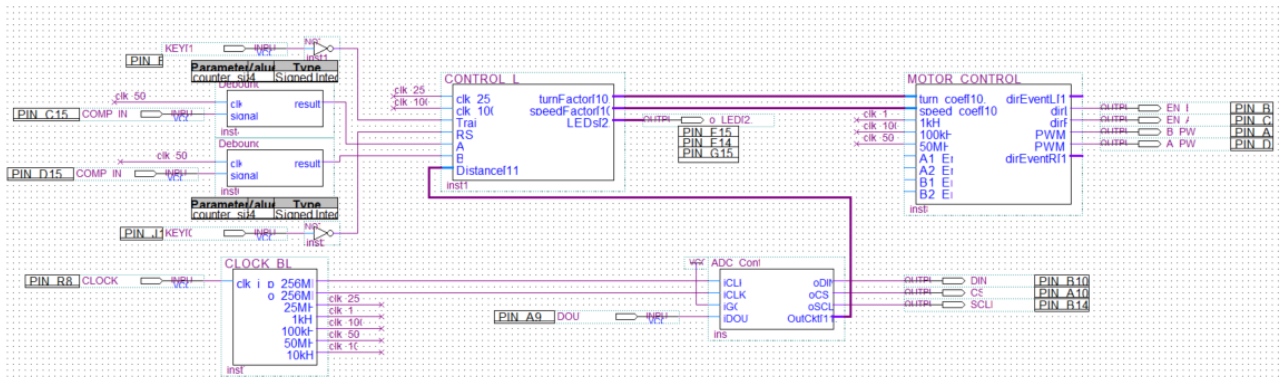


Fig. 18. Main design file of the controller circuit.

Logic flow goes from left to right, input signals from 2 coils enter the COMP_IN inputs, which are connected to debouncing block that waits for a certain period of time specified using generic value, right now the signal has to be longer than 42 us to pass through. After debouncer, signals enter the logic block, the diagram for which is shown in Fig. 19.

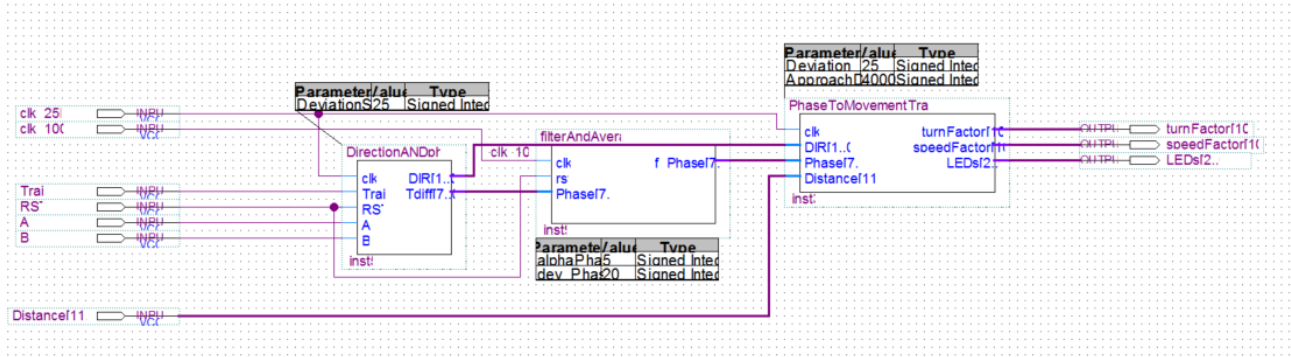


Fig. 19. Logic block inside the main design file.

In this block, control signals for motors are generated – turnFactor and speedFactor. Another output goes to LEDs. So, starting from left to right, first block logic generates the Direction and Phase outputs. Direction is given by three values (1, 0, and -1), where 1 represents right turning, 0 means no turn should be applied and the tank should go perfectly straight, and -1 represents left turning. Phase output does not represent the actual phase, instead, it's a counter based on a clock frequency of 25 MHz that measures the time difference between two successive rising edges. Since the frequency of the signal stays roughly the same, this counter is a good measure to base the tank movements on.

After conducting the experiments, it has been found that changes in temperature and surrounding magnetic field, change the phase result as well. To account for this, offset variable has been added to the program, so that when transmitter and receiver are on the same line, the phase result will be zero when offset is added.

The flowchart that explains how DirectionAndPhase block operates is in Fig. 20.

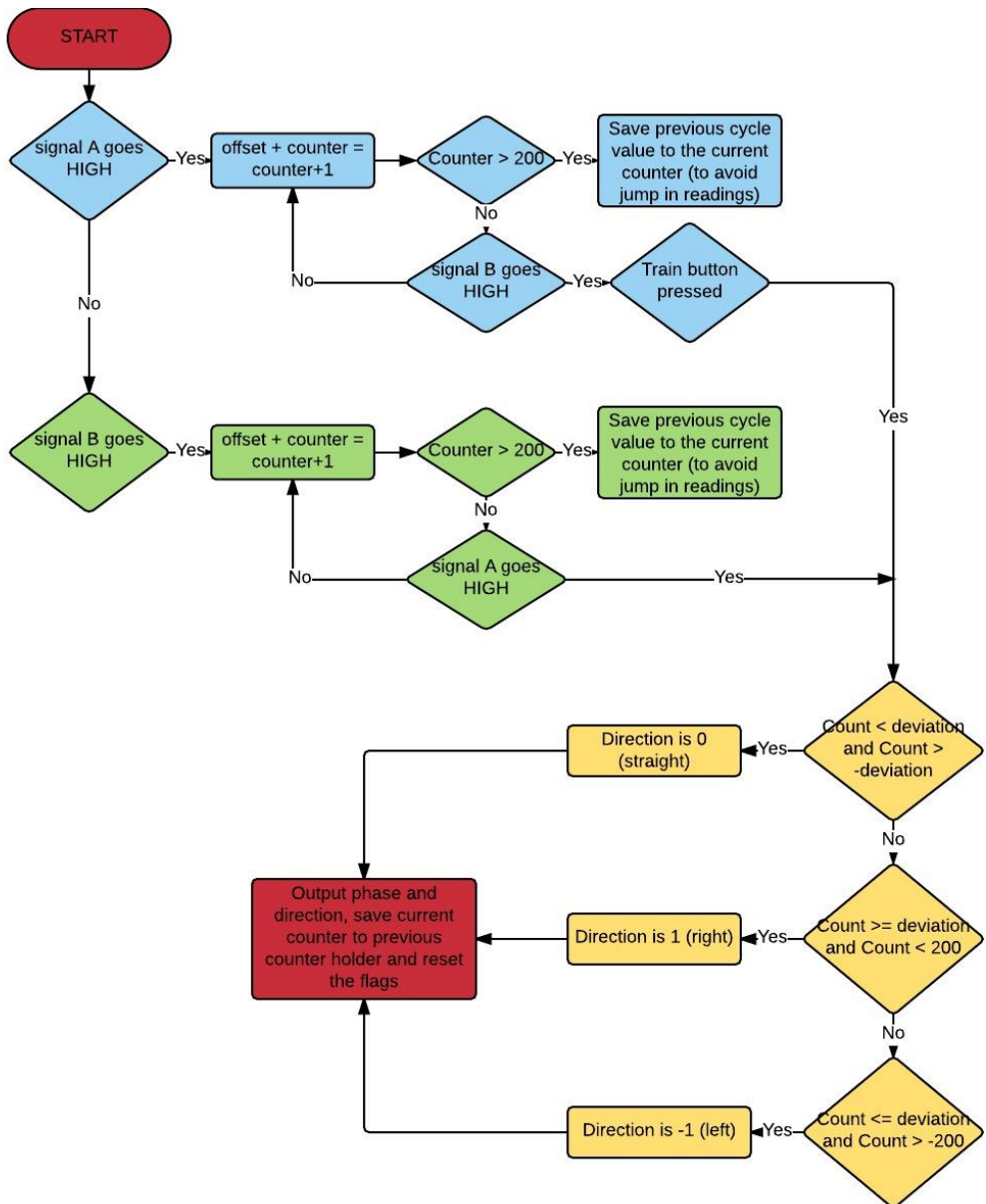


Fig. 20. Flowchart of the *DirectionAndPhase* block.

In the final version, deviation has been set to 50, to cover larger area and avoid flickering between left and centre or right and centre.

Next block is the *FilterAndAverage*, this block keeps a running average of the values and helps to reduce the spikes in the data. Flowchart for the internal logic of this block is shown in Fig. 21 (left).

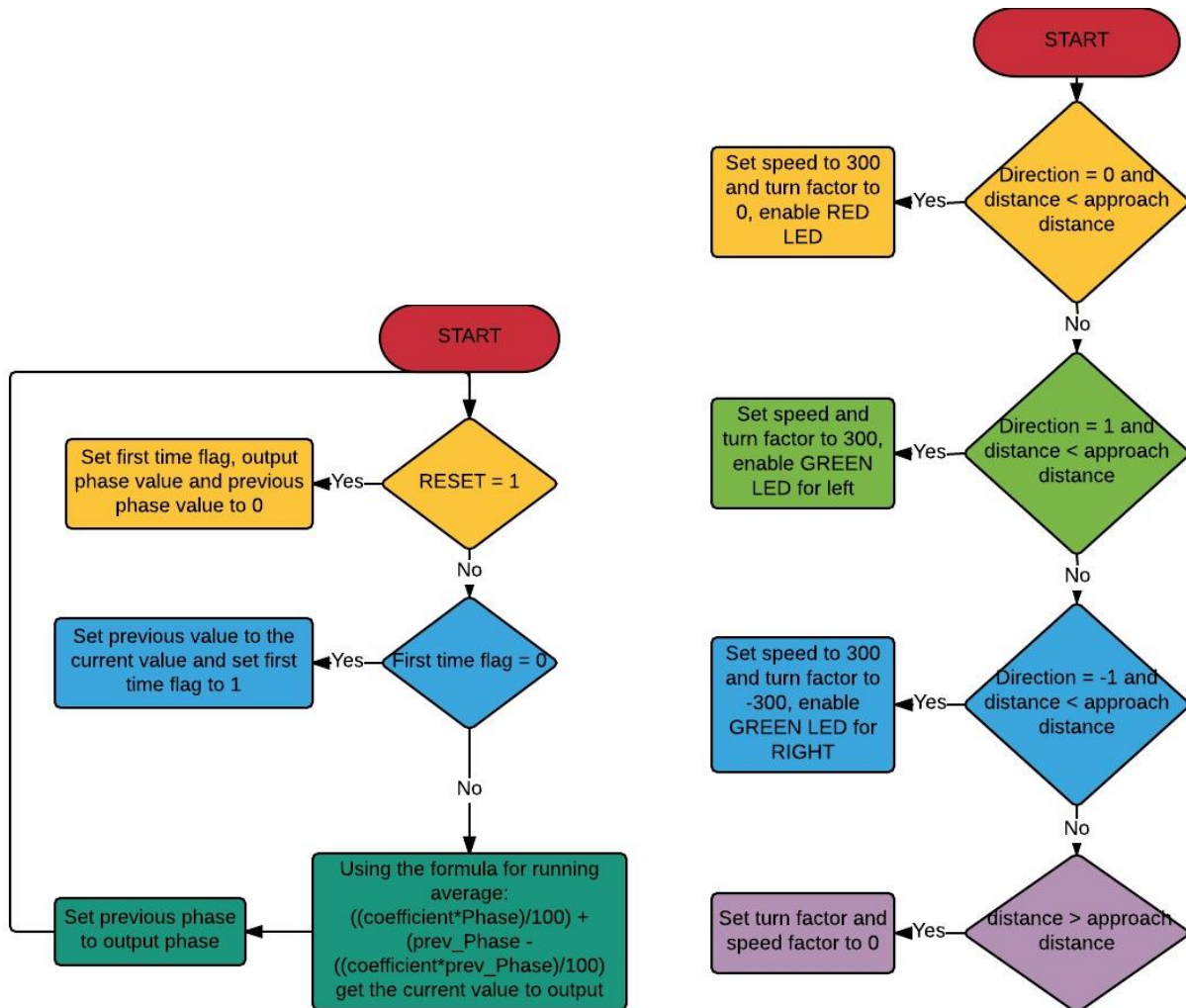


Fig. 21. *FilterAndAverage* block flowchart (left) and *PhaseToMovementTranslator* flowchart (right).

After averaging block, direction and phase go into *PhaseToMovementTranslator*. This block translates input phase into turn rate for the motors and depending on direction sign, tank goes left, right or straight. The logic for this block functionality is shown in Figure 21 (right).

The block that controls the motors is called M_CONTROL (copied from the AINT308 coursework), it accepts turnFactor and speedFactor. Internal structure of the block is shown in Fig. 22.

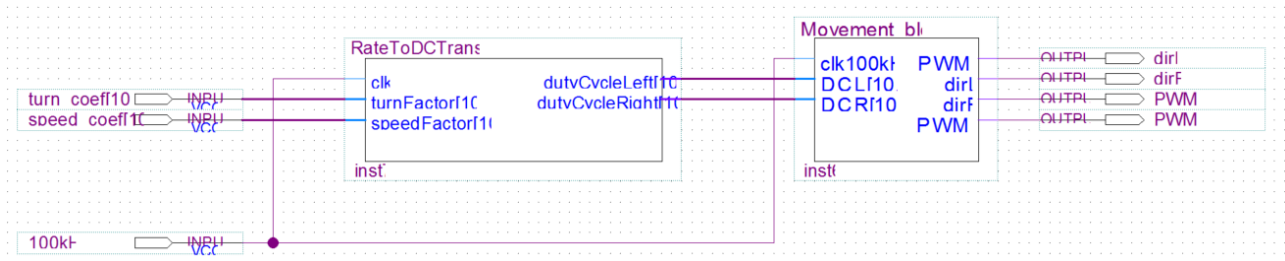


Fig. 22. Internal structure of the *M_CONTROL* block.

RateToDCTranslator block converts turnFactor and speedFactor to duty cycle for each wheel. Duty cycles are passed into Movement_block. The insides of the Movement_block are shown in Fig. 23.

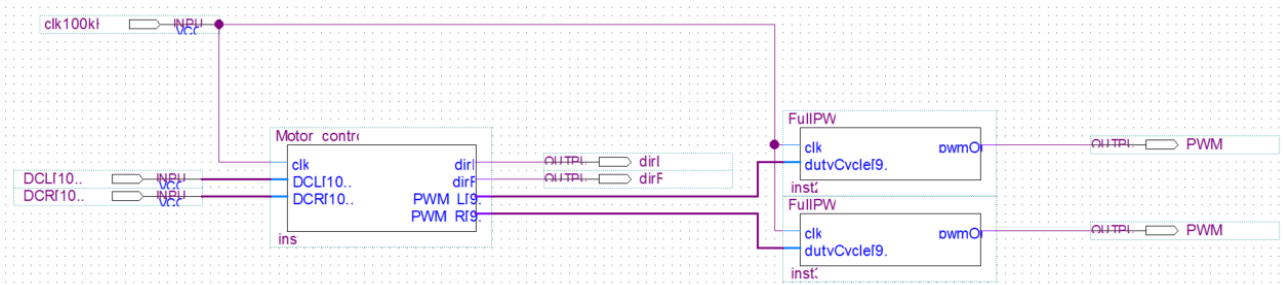


Fig. 23. Movement_block internal structure.

Motor_controller creates PWM signal and Direction signal from duty cycle input. After this, two directional signals are used to set the direction of the wheels. DutyCycle which is fed into FullPWM block is analysed and PWM signals for each wheel is generated.

7. ASSEMBLY AND TESTING

In this section different test types will be overviewed first. Secondly, detailed description of the tests conducted on each circuit will be shown.

7.1 Testing methods

This section covers details of the assembly of the circuits and coils and their testing as these two processes are intervened and basic testing has been done during the assembly.

PCB testing methods:

1. One of the first and basic methods of testing PCB is the visual inspection for short circuits and matching the actual traces to the schematic in Proteus software. This method allows one to reveal apparent mismatch in some cases and save time otherwise spent on soldering. Jumper wires are added to their places.
2. Continuity function on multimeter is used on a whole circuit to find misplaced connections with the size smaller than 10 thou (0.254 mm) which are not easily seen. Schematic is used for reference during the test.
3. Power stage is soldered in place and tested in regards to the output voltage.
4. Last stage means that all the components are soldered in place and continuity check is performed again, as during the soldering process drops of solder can cover the distance from pad to ground plane and cause short circuit. If that is the case this connection is desoldered or cut.

Circuit testing methods:

1. Send known waveform of pulse into the input and check if the output is within specified range.
2. If this is a controller board, write test program for each component to test it separately.

These two general methods have been used to test all the circuits with some small variations, more detailed explanation of tests for each component is given in respective sections dedicated to each of the components. Standard equipment such as oscilloscope Rigol DS1056, signal generator FeelTech FY3200S and batteries as a power supply has been used in most of the tests.

7.2 Excitation circuit testing

First phase of the test has been done using power supply to check the output voltage.

Input voltage	Output of LP2954	Output of Murata 0515SC
8 V	4.99 V	+14.99 V & -14.99
10 V	5 V	+15 V & -15
12 V	5 V	+15 V & -15

For testing the intermediate output stage, signal oscilloscope probes has been connected to the input stage of the op-amp for both signals. Three samples has been taken for reference:

Frequency (kHz)		Voltage (V)	
Signal 1	Signal 2	Signal 1	Signal 2
20.99	20.99	9.89	9.99
21	21	9.99	9.98
21.4	21.4	9.81	9.99

Output stage has been tested in the same manner to check the phase between signals and the output voltage as demonstrated in Figure 7.

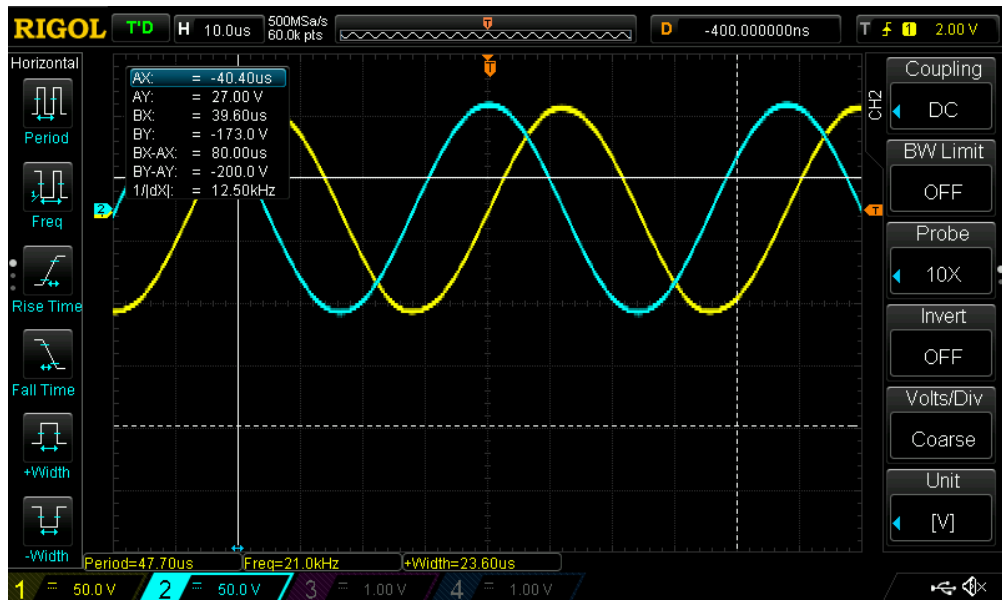


Fig. 24. Oscilloscope capture of the excitation circuit output.

To test the current that will be going through the coils, resistor with the value of $150\ \Omega$ was attached to the outputs of the op-amp in series with $1\ \Omega$ resistor. This procedure allows one to measure the current with oscilloscope. Expected value is around 133 mV peak-to-peak following the Ohms law: $10\text{V}/151\Omega = 0.066\text{ mA}$.

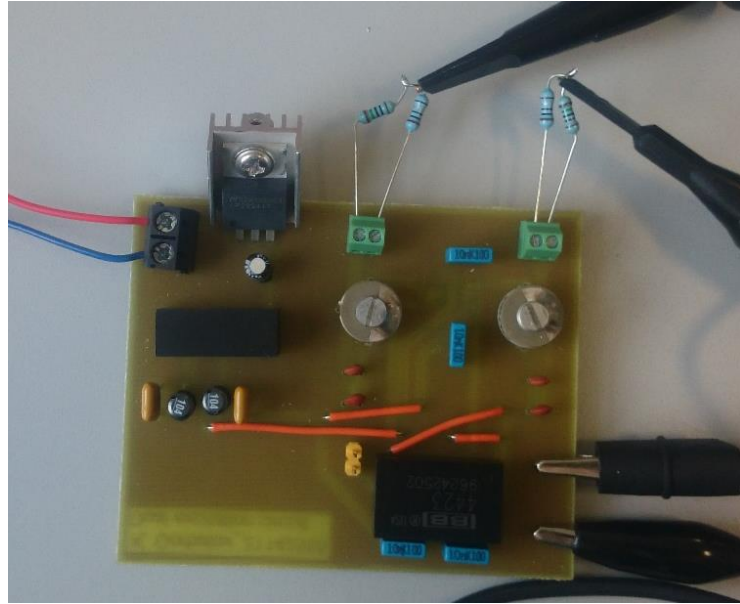


Fig. 25. Setup used to check if the op-amp functions properly.

After ensuring that the required current can be supplied, coils can be connected to the outputs for tuning. More details about tuning will be given in the appropriate section.

Table below shows all relevant characteristics of this circuit, including expected battery life:

Characteristic	Value and units
Total current consumption	224 mA
Total power consumption	2 W
Expected battery life (8 loop batteries fully charged)	5.9375 hours or around 5h if voltage drop after which battery could no longer be used is taken into account
Working input voltage range	29 down to 6
Output voltage	20 V peak-to-peak
Output frequency	$21\text{ kHz} \pm 500\text{ Hz}$
Output signals phase	90 degrees ± 10 degrees worst case

7.3 Power and Input circuit testing

This circuit does two things, it supplies all the circuits on the receiver side with power and it takes input signals from the coils passes it through tuning stage and feeds into filter. Therefore, each function needs to be tested individually.

Power stage output against input tests:

Input voltage	Output of LP2954	Output of Murata 0505SC
8 V	4.95 V	+5.46 V & -5.46
10 V	4.99 V	+5.44 V & -5.44
12 V	4.98 V	+5.45 V & -5.45

Stated output of the Murata 0505SC is ± 5 volts, but in reality when the regulator is not loaded by at least 50% of its stated load (200mA) it will have up to 10% added to nominal value as shown in Fig. 26.

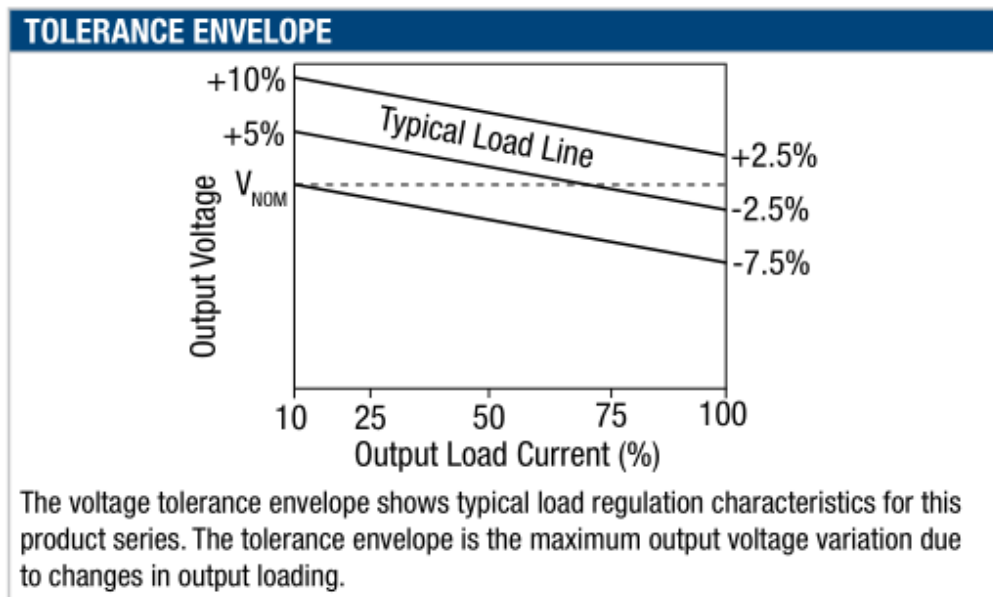


Fig. 26. Snippet from the datasheet showing the load vs voltage of the voltage converter.

Knowing that measured current consumption of filter (148 mA) and comparator circuits together is 64 mA. When both circuits are connected, voltage drops to 5.4 V. This fits with all circuits differential voltage threshold.

Signal input stage:

Input from the coils are fed through capacitors connected in parallel and goes to the op-amp configured as a voltage follower. To test this configuration, input and output signal voltage and phase are compared using oscilloscope. The result for coil 1, assembled first has been as expected and its tuned value depended on the value of variable capacitor. Coil 2 gave at least twice as less at any distance from the transmitter, and since all other parameters were the same, including resistance of 95 (Ohms) ferrite size and winding direction it has been assumed that the ferrite core is different. This assumption has not been tested, as it requires specialised equipment and extra time. To remedy this problem to some extent, the gain of 2 has been put for the weaker coil to provide the filter with similar values and possibly improve signal to noise ratio with this. Resistors used to get this gain is 1 kΩ according to the formula: $V_{in} = V_{out} \times R_1 / (R_1 + R_2)$. Giving the gain of 2 for two identical resistors. After assembling the rest of the receiver system, the voltage on the output of this circuit has been measured and plotted against distance, results are shown in Fig. 27.

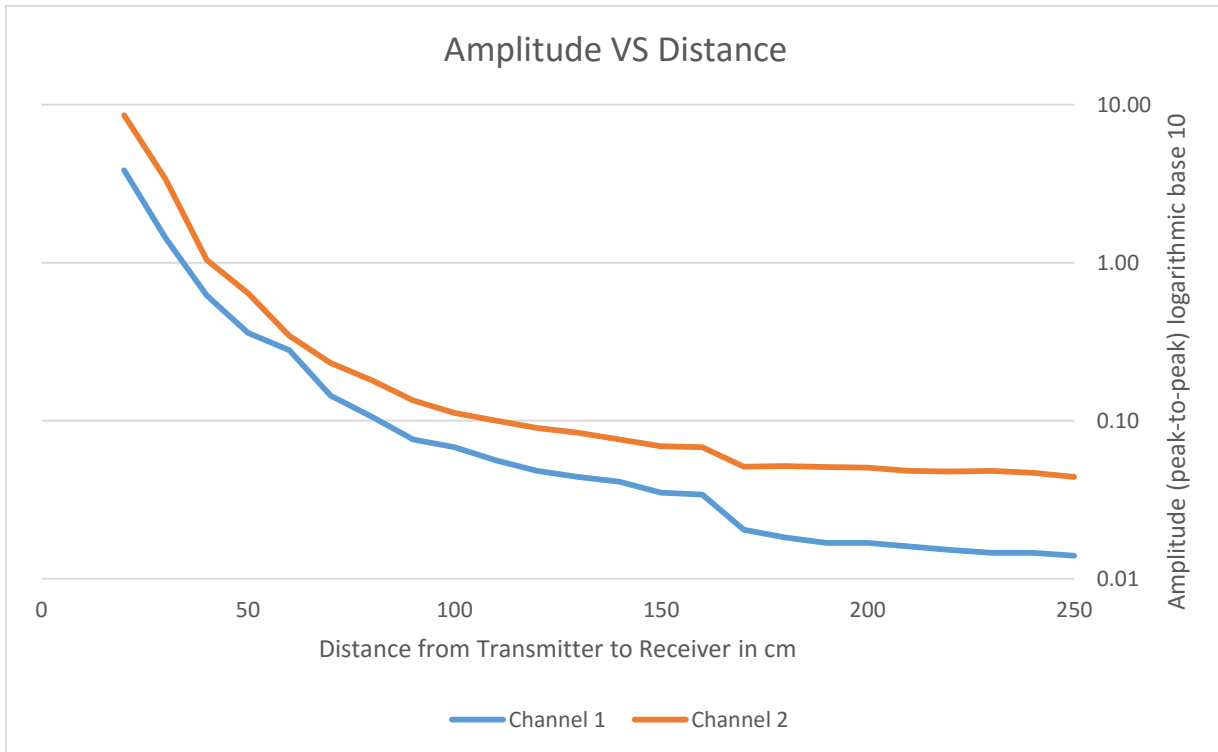


Fig. 27. Plot of the amplitude to distance relationship.

As can be seen from the chart in Fig. 27, 20 cm is the close limit until which the platforms can approach each other as the maximum that the operational amplifier can handle is 10 V peak-to-peak

but the actual near limit is even further. It has been found that the closest distance where the phase behaves linearly is 90 cm, as otherwise, the filter saturates and phase shifts. The far limit of the filter circuit boosting lies at about 250cm. However, in reality, the signal becomes too noisy for the filter to be able to distinguish the phase reliably. Fig. 28 demonstrates the level of noise at 100cm and 200cm for side-to-side comparison.



Fig. 28. Comparison for the level on noise at 100cm (left) and 200cm (right).

Therefore, while certain level of noise does exist at 100 cm, the main frequency and phase is still detectable. While at 200 cm, the noise populating the carrier wave becomes indistinguishable from the main frequency and the signal effectively disappears.

Concluding all stated above, ideal region in which current setup can operate, goes from approximately 90 to 170 cm.

The table summarising the main characteristics of the Input and Power circuit are given below:

Characteristic	Value and units
Total current consumption	64 mA
Total power consumption	0.66 W
Expected battery life (8 eneloop batteries fully charged)	8.3 hours (including the controller consuming 96.3 mA) or around 5.1 h if voltage drop after which battery could no longer be used is taken into account
Working input voltage range	29 down to 7

7.4 Filter circuit testing

Filter circuit has been tested using previously mentioned circuits: Excitation and input circuits. Signal with the amplitude of 10V from excitation circuit has been passed through the voltage divider and the values were:

R1	R2	Expected output voltage (mV)
10 K	100	100
18 K	100	50
45 K	100	20
90 K	100	10

Actual values recorded for first and second channels are below:

	Input voltage (mV)	Output voltage (mV)
Channel 1	30.4	2000
	56	4200
	108	8800
	216	11200
Channel 2	28.8	1720
	44	3600
	96	7800
	192	10800

Plot of these values is given below in Fig. 29.

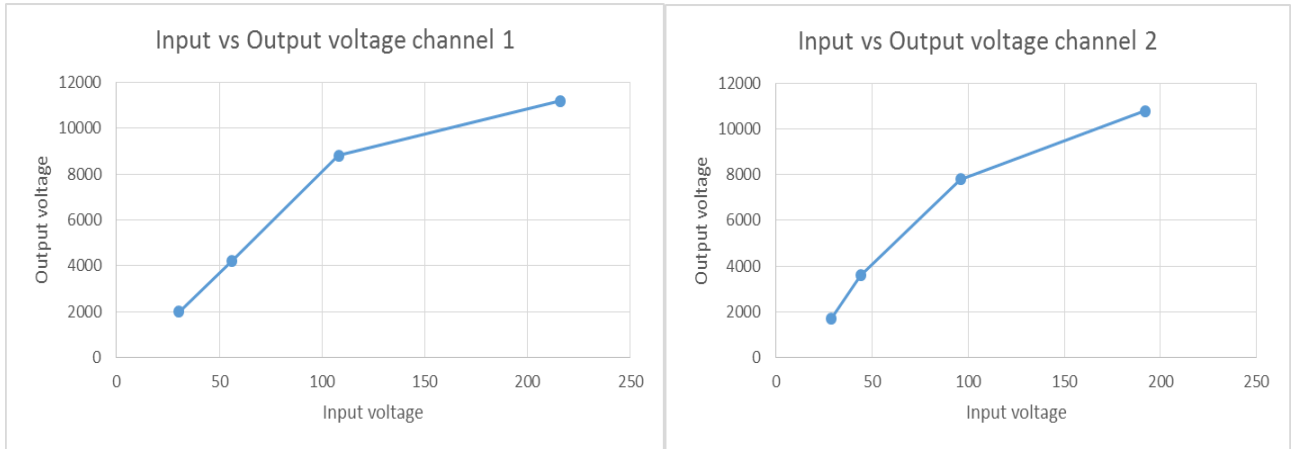


Fig. 29. Channel 1 and Channel 2 input and output voltage relation.

As can be seen in Fig. 29, relationship between input and output voltage is almost linear, small variations can be explained by noise in the oscilloscope existing for small signals and resistor intolerances.

Second stage is to test the quality of the filter relative to its central bandpass frequency of 21 kHz. For this, the filter has been connected to input and power circuit which in turn connected to the waveform generator. Generator produced sine wave on both channels with a shift of 90 degrees, the start frequency was 16kHz and end frequency was 26kHz. The table with values is shown below:

Channel 1		Channel 2	
Frequency	Amplitude	Frequency, kH	Amplitude
16	3	16	10
16.5	5	16.5	10
17	5	17	10
17.5	10	17.5	10
18	27	18	30
18.5	88	18.5	100
19	404	19	483
19.5	1800	19.5	1810
20	1900	20	1830

20.5	1830	20.5	1700
21	1720	21	1540
21.5	1600	21.5	1440
22	1360	22	1290
22.5	1100	22.5	955
23	408	23	342
23.5	87	23.5	100
24	40	24	40
24.5	10	24.5	20
25	10	25	9
25.5	5	25.5	5
26	5	26	5

Plot of these values as well as theoretical response is given in Fig. 30.

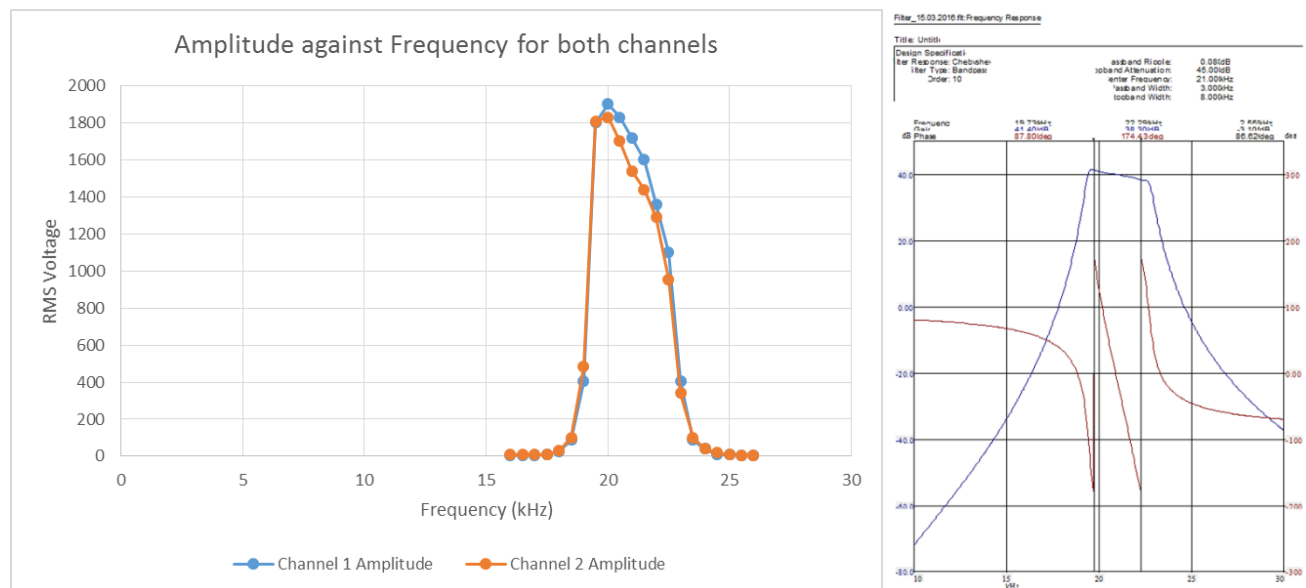


Fig. 30. Bandwidth response of the filter against predicted graph.

Comparing the shape of the resultant graph with the prediction given by Linear Technology tool it can be concluded that the filter works as expected.

Last test is conducted to test the consistency of phase at different frequency. Setup is the same, only this time phase is monitored. Frequency values and approximate phase is shown in the table below

Frequency (kHz)	Phase (Degrees)
18.5	80-95
19	80-85
19.5	73-78
20	77-83
20.5	79-89
21	84-87
21.5	89-93
22	88-92
22.5	87-90
23	95-100
23.5	87-92

Table above shows that phase tend to vary with frequency by ± 10 degrees from 90 degrees. This investigation will help with phase threshold tuning for tank platform.

7.5 Comparator circuit testing

Comparator has been tested using signal generator and filter circuit output. First tests has been done using signal generator to test the output voltage.

Input voltage (peak-to-peak)	Comparator output (0 to 5V)	
	Channel 1 (V)	Channel 2 (V)
10 V	4.98	4.97
8 V	4.99	4.89
5 V	5	5
2 V	4.98	5

As expected, the voltage on the output square wave stays constant, as it is driven from the separate power pin. For the second test, comparator has been connected to the filter to get the real world data in regards to noise and correct transitions. Data from different angles has been plotted against phase measured using the cursor on a oscilloscope. Resultant graph and data are shown in Fig. 31.

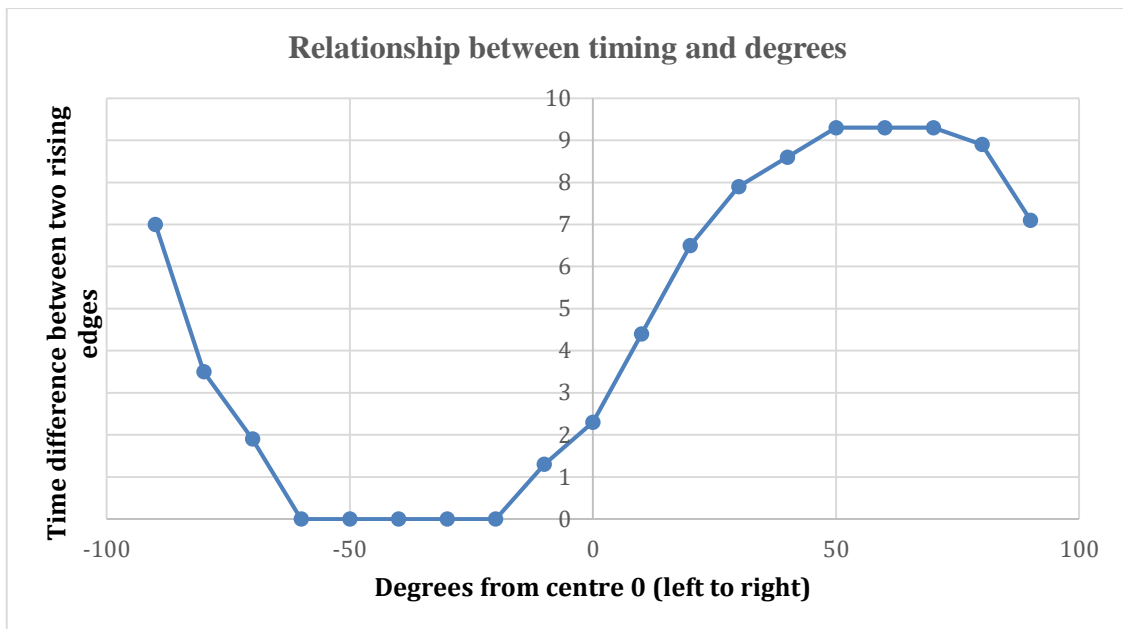


Fig. 31. Graph showing relationship between time difference and angle of the receiver.

Timing column means that the difference between two rising edges has been measured and time difference between them calculated. The resultant graph on Fig. 31 corresponds to theoretical behaviour of the sensor.

7.6 Controller circuit testing

Controller testing will be performed in two steps, hardware and software testing.

7.6.1 Hardware testing

Controller testing involves testing of peripherals in how they correspond to expected values as well as the algorithm test on FPGA.

Logic level shifter test (5 V to 3.3 V):

The test has been done on a separate breadboard to ensure that its performance is sufficient for the task before soldering it in place. The picture of the setup and the oscilloscope output is shown in Fig. 32.

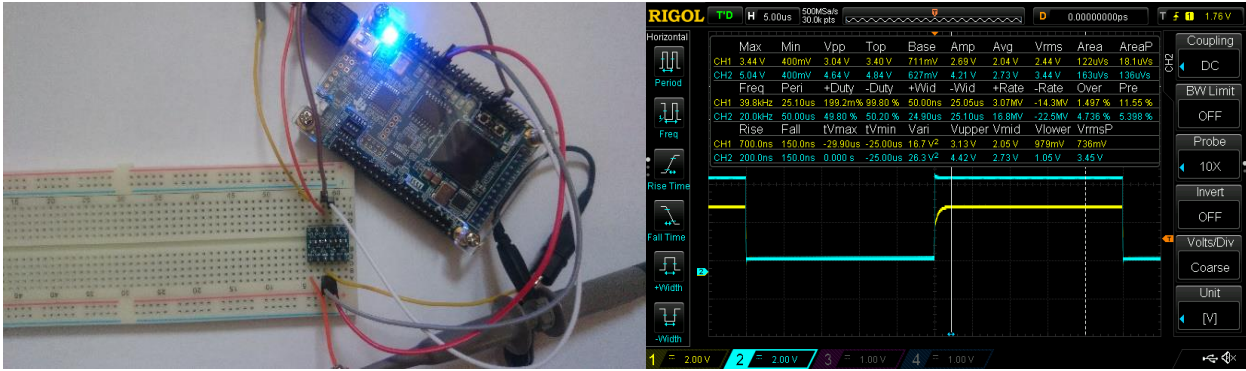


Fig. 32. Logic level shifter setup and oscilloscope output.

Fig. 32 shows how the form of the wave changes after passing through the logic level shifter represented with yellow line. Blue line is the input to the chip. To ensure that the smoothed edge does not affect the performance, the output has been tested using DEO-NANO. Fig. 33 shows the resultant signal received.

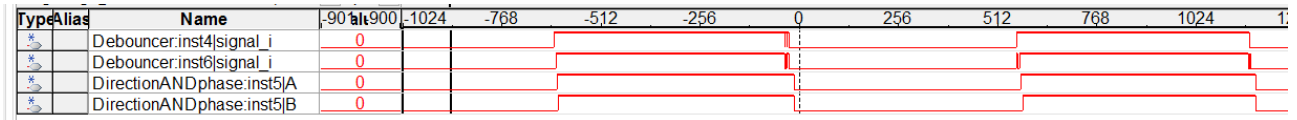


Fig. 33. SignalTap output of two waveforms before and after debouncing.

SignalTap software has been used to produce this result. It works in a similar way to logic analyser, except that it takes a signal directly from the inside the FPGA and transfers it through USB cable to the computer.

Debouncer:inst4|signal_i is the input A while Debouncer:inst6|signal_i is B. From Fig. 33 it can be concluded that the logic analyser is a suitable chip to use. As for the noise in the input, it can be effectively negated using the debouncer block, also used for the encoders and buttons. Debouncer main algorithm is to take the input and measure how long it lasts, if it lasts longer than the set threshold, debouncer allows the signal to pass. If not, the signal level before the logic level change is maintained.

Analog-to-Digital (ADC) converter test

ADC allows to sample analog signals at specified periods of time and by doing this, make them discrete and readable by FPGA. ADC converter on DEO-NANO is ADC128S002 that can sample at speeds from 0.8 to 3.2 MHz.

As a guideline for creating the code to drive the ADC chip the documentation by Terasic technology has been used. To test the module, signal generator has been hooked up to the input pins on DEO-NANO, illustrated in Fig. 34.

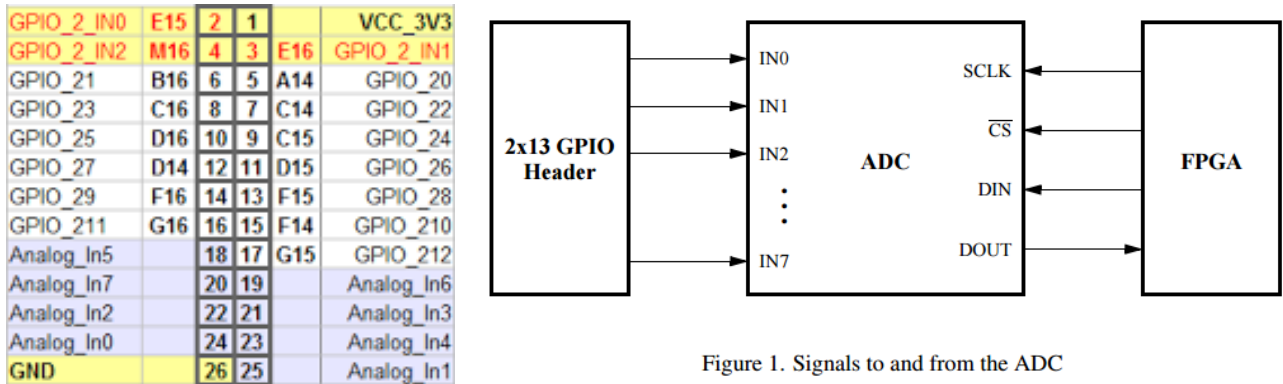


Figure 1. Signals to and from the ADC

Fig. 34. 2x13-header pinout for analog inputs of the adc converter [14] and general schematic for the chip i/o [15].

The result of the 2 channel test with channel 0 being grounded and channel 1 connected to the internal 3.3V supply on DEO-NANO is shown in Fig. 35.

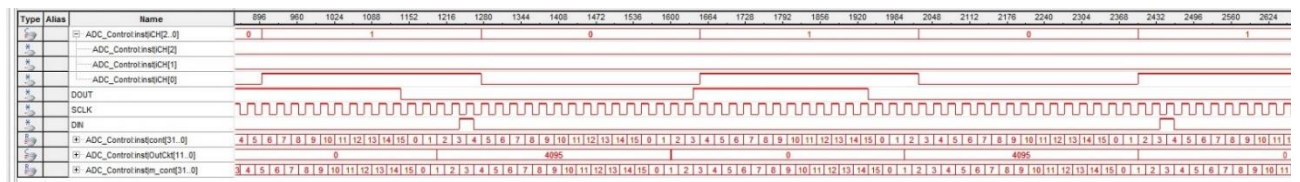


Fig. 35. ADC test with both channels monitored, constant dc voltage.

OutCkt is the output of the logic block in the form of the vector array. 4095 indicates that 3.3 volts is achieved while 0 is the ground.

To test the ability of the ADC chip to handle alternating signal on multiple inputs, another test has been done with signal generator connected to channel 0 and channel 1. The result is shown in Fig. 36.

Type	Alias	Name	1024	-768	-512	-256	0	256	512	768	1024	1280	1536	1792	2048	2304	2560	2816	3072	3328	3584	3840	4096	
		Phase:inst4[Decipher:instclk]																						
		+ Phase:inst4[Decipher:inst channel[2..0]	1	0	1	0	1	0	1	0	1	0	1	0	1	0	1	0	1	0	1	0	1	
		+ Phase:inst4[Decipher:inst curValA[12..0]	155	121	994	2015	1218	121	905	2016	414	51												
		+ Phase:inst4[Decipher:inst curValB[12..0]	447	1768	1751	413	446	1767	1752	414	154	1110												
		+ Phase:inst4[Decipher:inst Wave[11..0]	121	1768	904	1761	2015	413	1218	446	121	1767	905	1752	2016	414	154	514	1110					

Fig. 36. SignalTap output for multiple signal sampling

When channel 0 and channel 1 were fed from same output of the signal generator the resultant waveform looks as shown in Fig. 37.

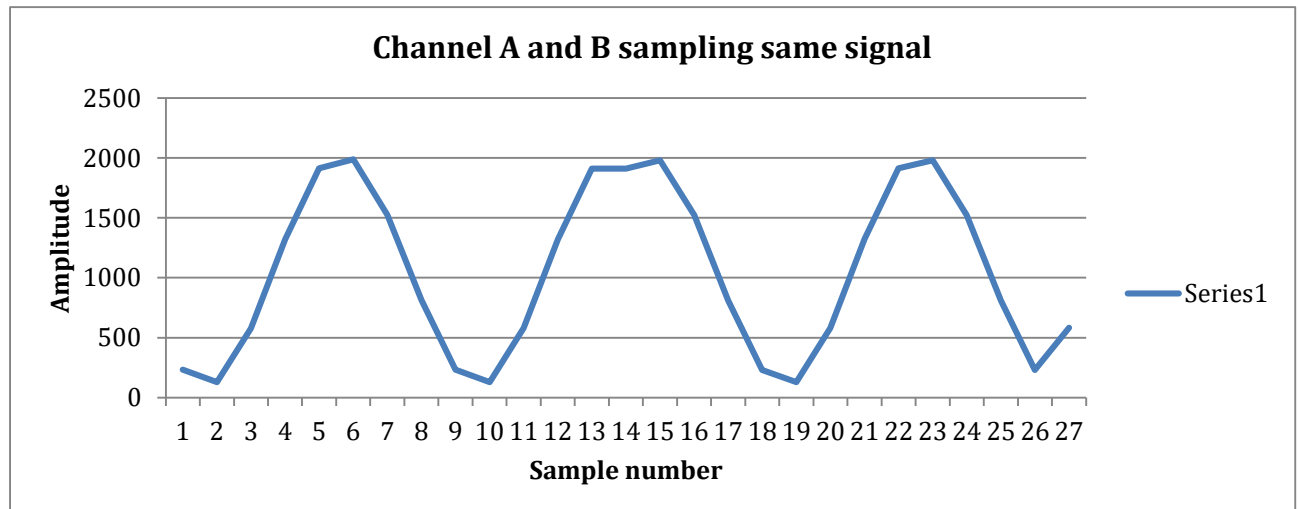


Fig. 37. Result of sampling single input with both channels.

Since the input to the ADC has been sinusoidal wave at 21 kHz, the result look close to reality with 8 sampling points per wavelength. When two different waves were fed to channel 0 and channel 1, the result became less accurate as shown in Fig. 38.

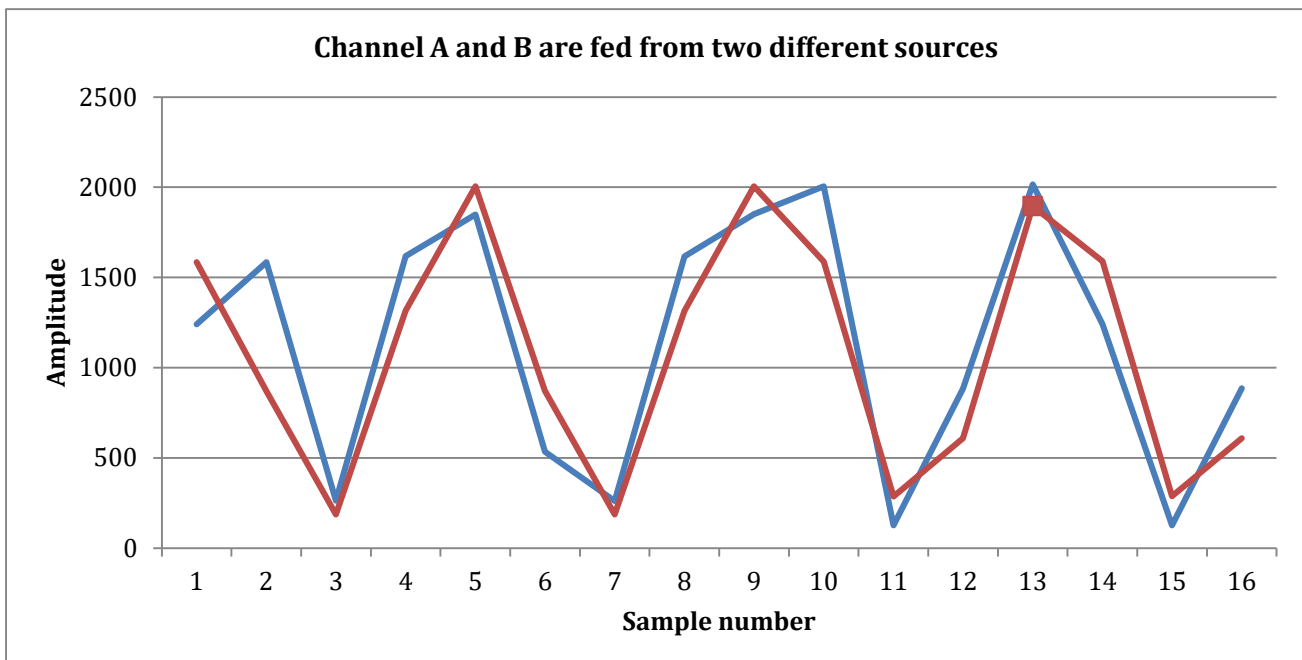


Fig. 38. Result of sampling two inputs with same phase with two channels.

Now, the sampling rate for each wave is twice as less and only four sampling points is allocated per wavelength but general shape is still recognisable. Overall, for the task of sampling the infrared sensor that has the output frequency of 21 to 28Hz the resolution is more than sufficient.

Infrared sensor test

Sensor model used in this case is Sharp GP2Y0A02YK0F with effective range 20 to 150cm. The graph for the sensor in datasheet is presented on Figure 39 taken from [12] and [13] sources.

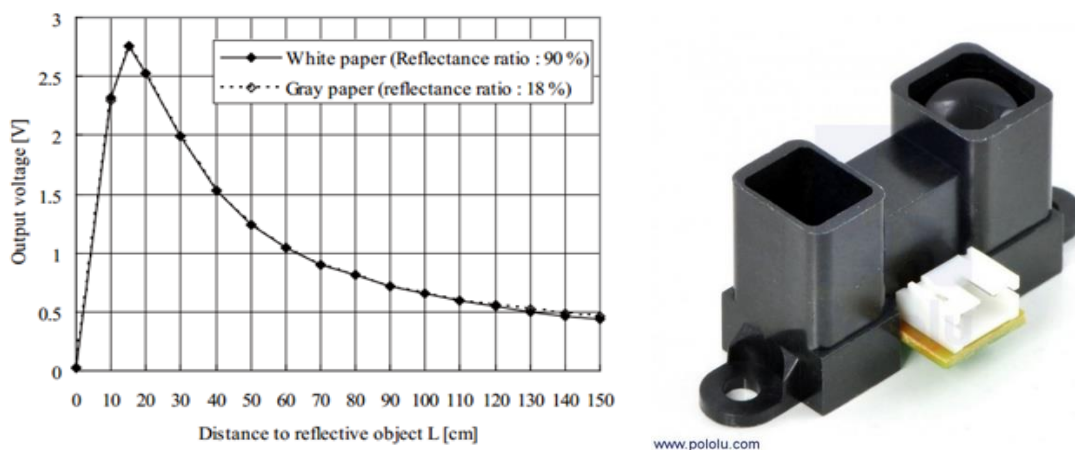


Fig. 39. Graph from the sensor datasheet and the sensor itself.

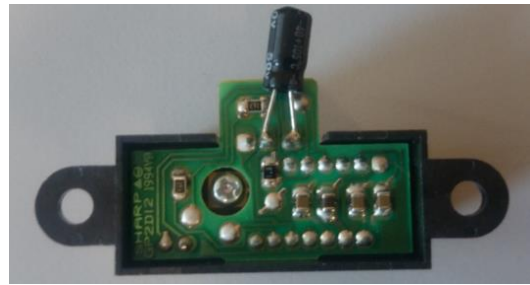


Fig. 40. Back panel of the sensor with capacitor across power leads.

As can be seen in Fig. 39, the curve within specified range is almost linear, with a small dip in the region from 40 to 80 cm. During the initial tests, it has been discovered that the sensor has a periodic spikes in its data output. After a short research for the information regarding this problem, the source of the problem has been found to be the power surge during some internal operations. To fix this, a relatively large capacitor of the value 1uF has been soldered across terminals to ensure that enough power will be available at all times. End result is shown in Fig. 41.

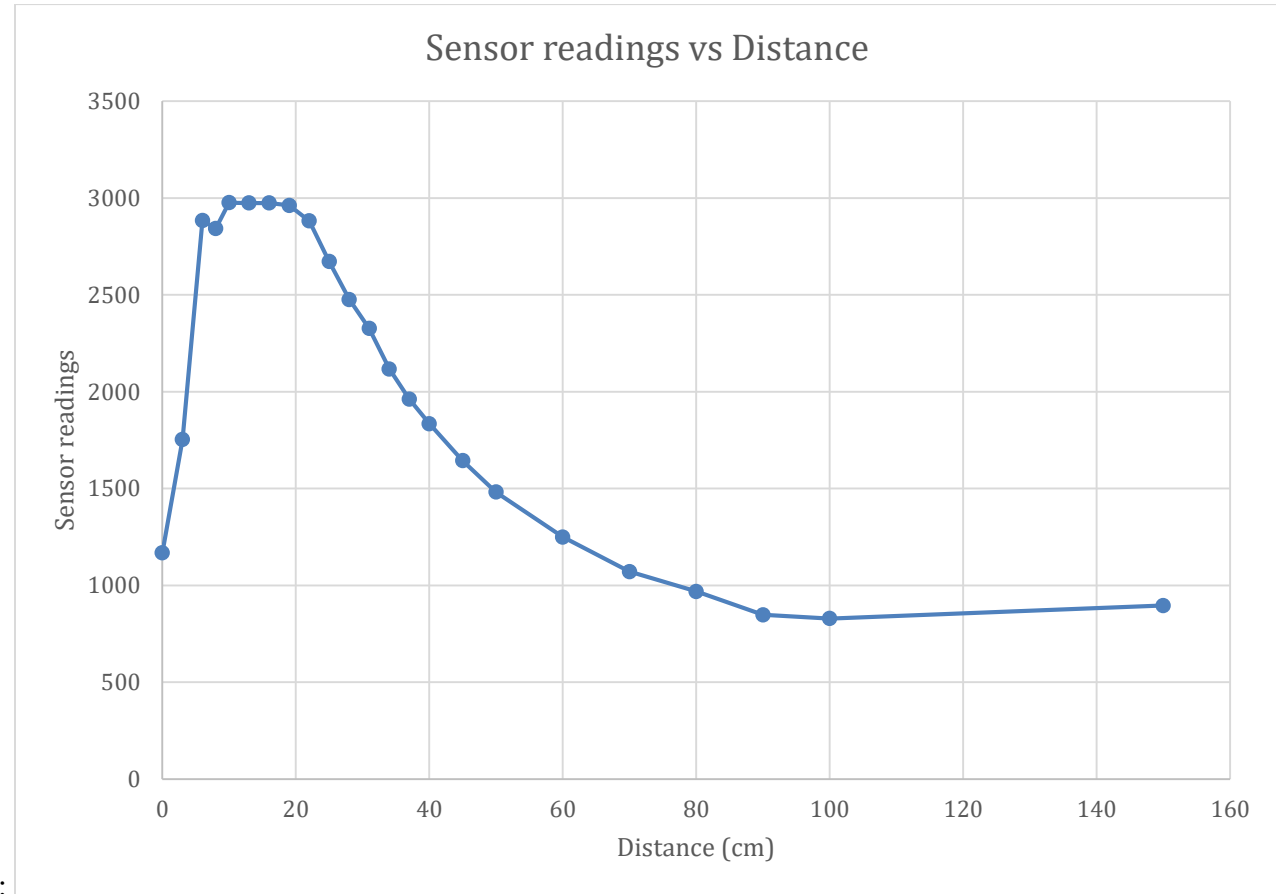


Fig. 41. Linearity graph representing sensor readings against distance to the object.

As can be seen from the graph, the datasheet and real world data matches and sensor performs as expected.

Motor driver test

To test it a simple test program has been written to change the direction and speed of the wheel rotation depending on the phase difference between signals. This allowed to simulate the effect of the real data coming from the receiver coil. In this case signal generator has been connected to the inputs of the logic level shifter and the following table with a graph has been obtained.

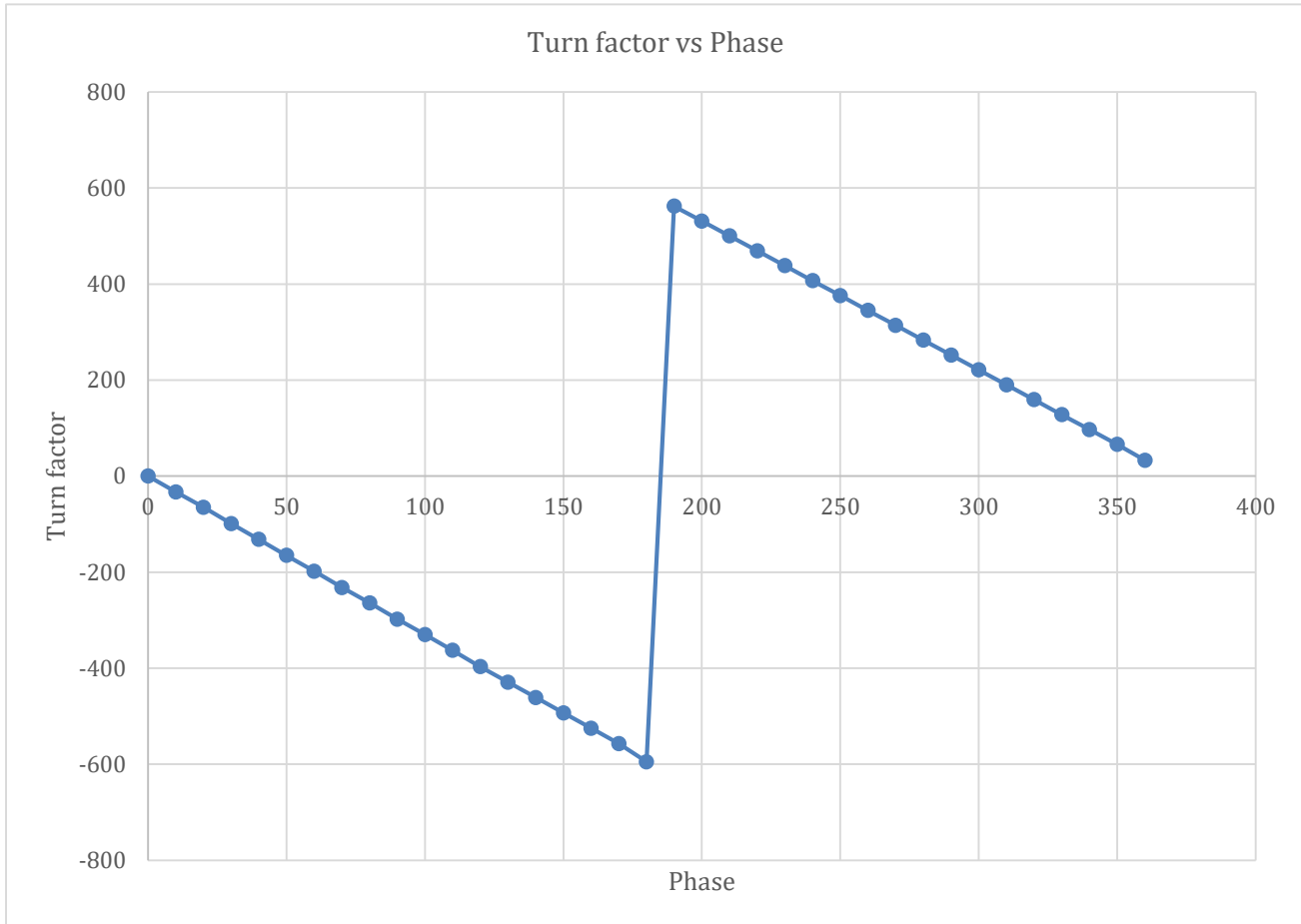


Fig. 42. Graph of Turn factor value against input phase into the controller.

Turn factor amplitude indicates the proportional speed of the wheel, so irrespective of the sign, the larger the number of turn factor – the faster wheel will spin. The sign of it indicates the direction of the turn of the tank. It has been found that the motor tends to affect the phase of the signal even after the bottom of the tank has been shielded with a copper tape, so the speed has to be kept low, at 1/3 of the maximum value.

LEDs test

Has been done in conjunction with other logic, so that when the sign of the phase is positive, LED number 3 is lit (green), if its negative, LED number 1 is lit (green) and if it's straight – LED number 2 is lit (red). SignalTap test results is shown in Fig. 43 below.

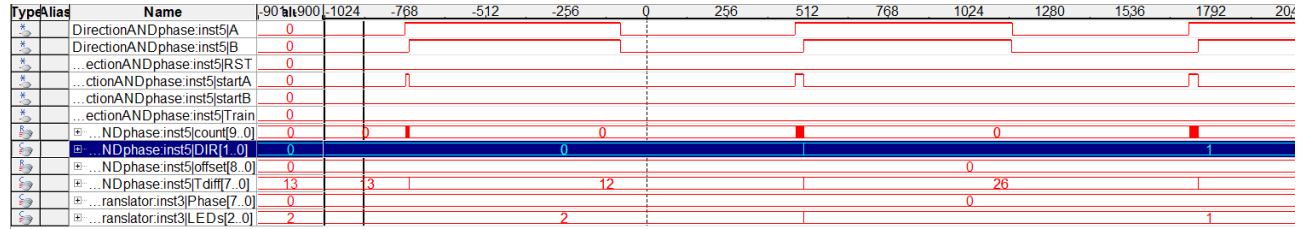


Fig. 43. Transition from right to center, numbers are in unsigned decimal.

On a Fig. 43, the LED variable is at the bottom. For convenience, one variable of type standard logic vector is used to drive either of 3 LEDs. So that each LED is represented as 1 in a bit vector of “000”. So that if vector is equal to “010” central LED is lit.

DEO-NANO testing

FPGA works reliably both using USB as a power source and using external power source of 5V. Logic output does not need testing as the device has been tested numerous times during the period of the course and the project.

7.6.2 Software testing

The first test has been done on the input signals, the source of the signals is the comparator. The signals have been sampled using SignalTap before the debouncer and after, to compare the quality of final signal. Result of the SignalTap is shown in Fig. 44.

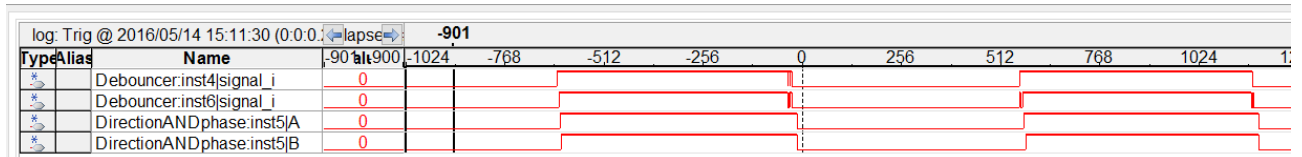


Fig. 44. SignalTap output from two signal sampling before and after debouncer.

Next stage is to test the counter and direction output of the DirectionANDphase with relationship to the angle of the transmitter to the receiver. Counter values have been plotted against angle for 3 different distances, as shown in Fig. 45.

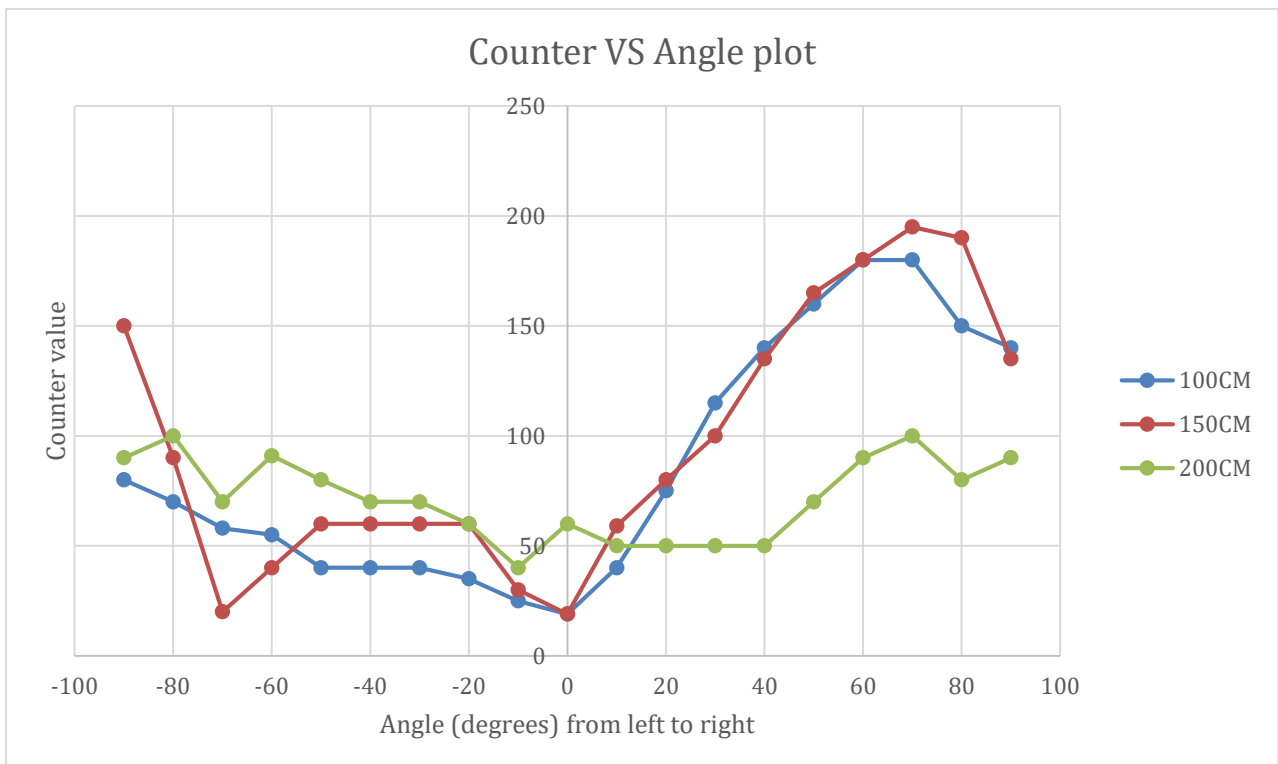


Fig. 45. Plot of the counter value against angle and distances.

Graph in Fig. 45, shows that the left side of the receiver respond to the changes in the orientation much less than the right side. When tested within ideal region, as defined in the test section for [Comparator circuit](#), the right side behaves linearly until 70 degrees, after which it goes decreases, therefore, making the detection of 40 and 90 degrees impossible. The left side is linear only for 20 degrees from the beginning, after which it stops responding to the further angle changes. However, the output is relatively stable even in this region, making it possible to detect at least the sign of the phase (which wave goes first) so for the purposes of following it is a minor disadvantage. When tested for the further distance, 200 cm, linearity vanished and the counter oscillated as much as by 45 degrees, which is a clear indicator that the noise level it too high.

In the ideal region, directional flag, which is used to determine the sides, behaved as expected, showing right and left sides reliably for the most part.

Since the current implementation of the code uses only directional flag to turn left or right, the testing has been as simple as rotating the platform left or right and checking that the LEDs approximately correspond to the left, right or centre.

8. CONCLUSIONS

The Kalmus guidance method has been successfully implemented using modern hardware and software. Coils have been tuned to transmit maximum power for transmitter and receive maximum power for receiver. Filter works as expected and mitigates most of the noise in the given distance region. FPGA, which has been used as a controller, drives the motors according to the sign of the phase between two signals. As a result, receiver platform is able to follow the transmitter platform over the distance from 1 to 1.7 meters, automatically correcting itself in regards to heading.

The tests have been done on all the components of the system to verify the correct performance and find potential problems.

Initially, several assumptions have been made. One of the main ones is the usage of the 21 kHz chip for the oscillator and the operational amplifier with a limit of 70mA for each of two channels. The decision to use 4423 oscillator has been due to its compactness and relatively good frequency stability. Operational amplifier that has been used was chosen due to its high power, internal power consumption and wide input voltage range. Also, since power converter limit is 2W, total power that can be used is limited.

The problems that have been found are the following:

- Receiver coils have different potential for receiving electromagnetic force due to differences in ferrite rods.
- Filter accepts too much noise due to relatively wide bandwidth.
- Due to absence of nu-metal shielding the noise from the motors and circuits affect the receiver coil readings.

Possible improvements for the project:

- Decrease the bandwidth of the filter.
- Add nu-metal shielding to the bottom of the receiver platform.
- Use voltage converter with larger power limit to avoid heating problem.
- Find ready wound coils to ensure that received electromagnetic force is equal for both coils.
- Add Schmitt triggering before comparator to fix the extra bounces in the signal.

Assembled platforms pictures are available in [10.5 APPENDIX 5: Final result](#)

9. REFERENCES

- [1] Faraday's law: https://en.wikipedia.org/wiki/Faraday%27s_law_of_induction
- [2] Motion tracking solutions from Polhemus (<http://www.polhemus.com>):
<http://polhemus.com/applications/electromagnetics>
- [3] F. H. Raab et al., “*Magnetic position and orientation and tracking system*”, IEEE Transactions on Aerospace and Electronic Systems, Vol. AES-15, pp. 709–718, (1979).
- [4] H. P. Kalmus, “A New Guiding and Tracking System”, IRE Transactions on Aerospace and Navigational Electronics, Vol. 9, pp. 7–10, (1962).
- [5] Exposure limits of electric and magnetic fields: <http://www.hydroquebec.com/fields/limites-exposition.html>
- [6] ATAN 2(y, x): <http://en.wikipedia.org/wiki/Atan2>
- [7] American Wire Gauge (AWG) Cable/Conductor Sizes:
<http://diyaudioprojects.com/Technical/American-Wire-Gauge>
- [8] Q-factor: https://en.wikipedia.org/wiki/Q_factor
- [9] Wireless power transfer: https://en.wikipedia.org/wiki/Wireless_power_transfer
- [10] Filter CAD from Linear Technology: <http://www.linear.com/designtools/software/#Filter>
- [11] Quadrature oscillator: <http://www.ti.com/lit/ds/symlink/4423.pdf>
- [12] Measure distances from the Sharp GP2Y0A02YK0F sensor using an MCP3008 ADC and hardware SPI: http://jeremyblythe.blogspot.co.uk/2012_09_01_archive.html
- [13] Sharp GP2Y0A02YK0F Analog Distance Sensor 20-150cm:
<https://www.google.co.uk/url?sa=i&rct=j&q=&esrc=s&source=images&cd=&cad=rja&uact=8&ved=0ahUKEwiA74Hm8XMAhXkJMAKHVvBAJIQjRwIBw&url=http%3A%2F%2Fcore-electronics.com.au%2Fsharp-gp2y0a02yk0f-analog-distance-sensor-20-150cm.html&psig=AFQjCNHd3mfPIEEAKGHCUg37g0boq5MbqA&ust=1462614922035834>
- [14] DE0-Nano | easier pinout: <https://sites.google.com/site/fpgaandco/de0-nano-pinout>
- [15] Using the DE0-Nano ADC Controller:
ftp://ftp.altera.com/up/pub/Altera_Material/12.1/Tutorials/DE0-Nano/Using_DE0-Nano_ADC.pdf

10. APPENDICES

List of appendices:

1. Mechanical drawings for components
2. Full sized circuit diagrams
3. Datasheets
4. Project materials and cost full graph
5. Final result

10.1 APPENDIX 1: Mechanical drawings for components

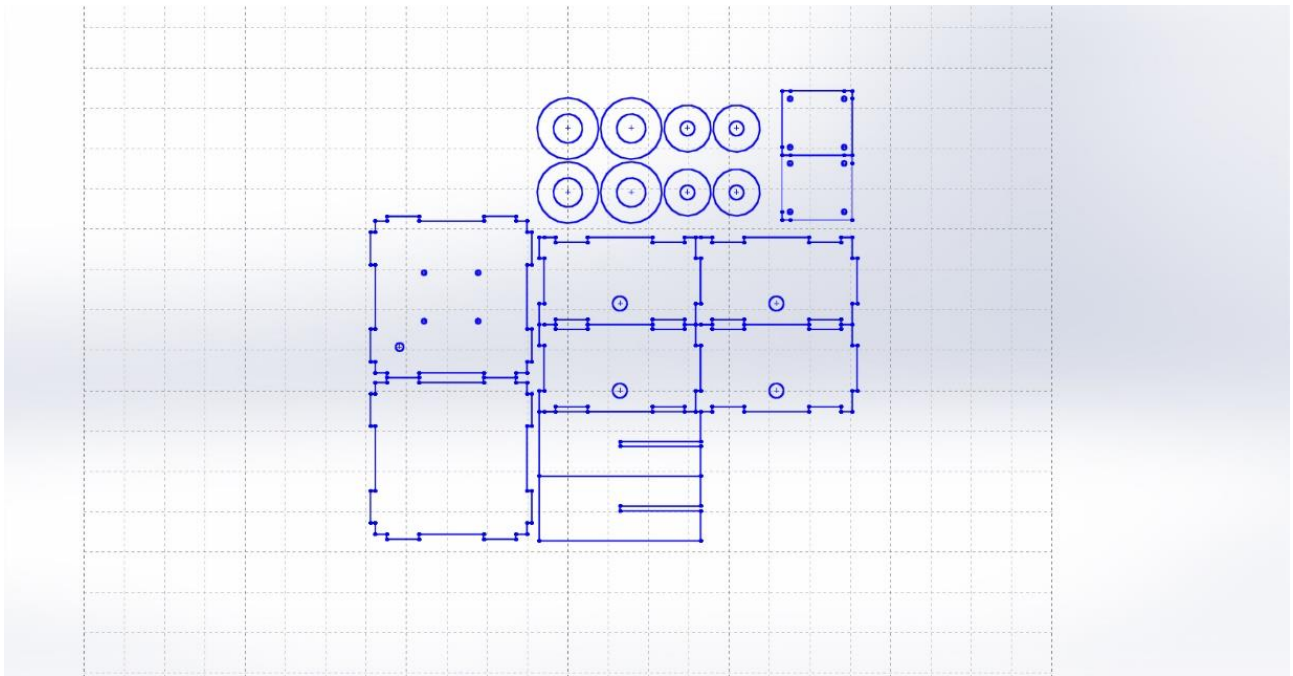


Fig. 1. Receiver box with the end caps for transmitter coils and new pole for the transmitter box.

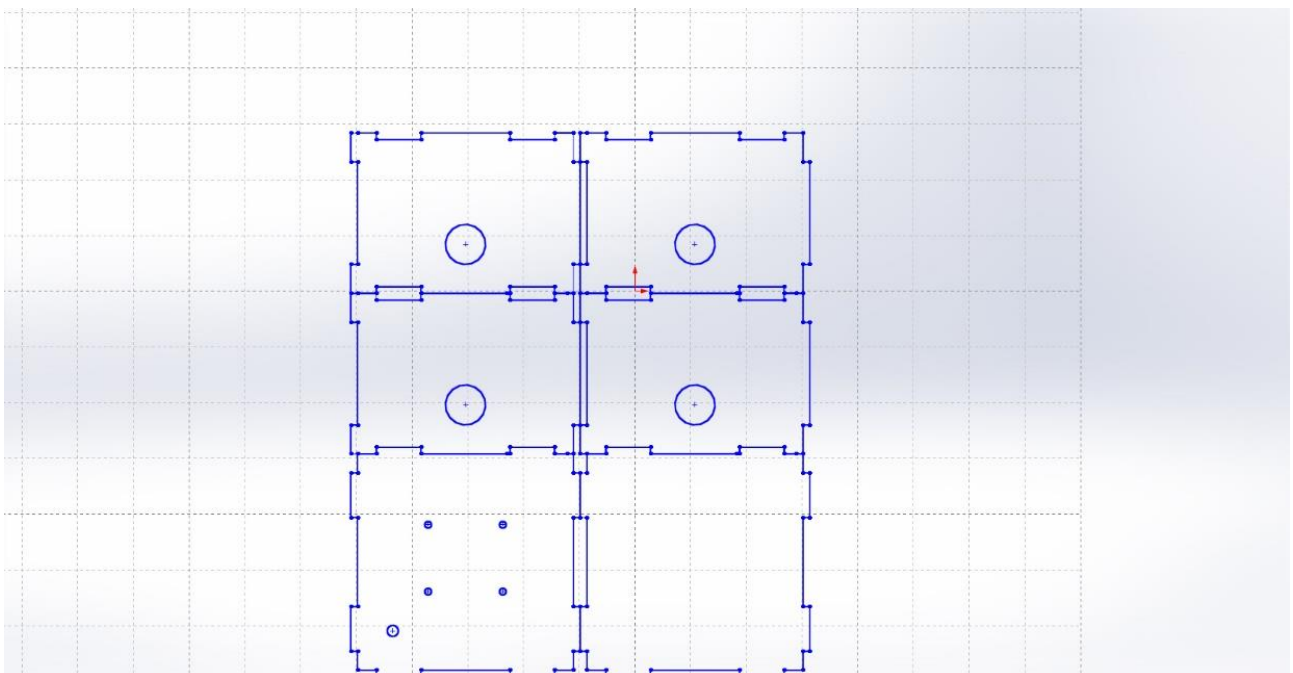


Fig. 2. Transmitter box.

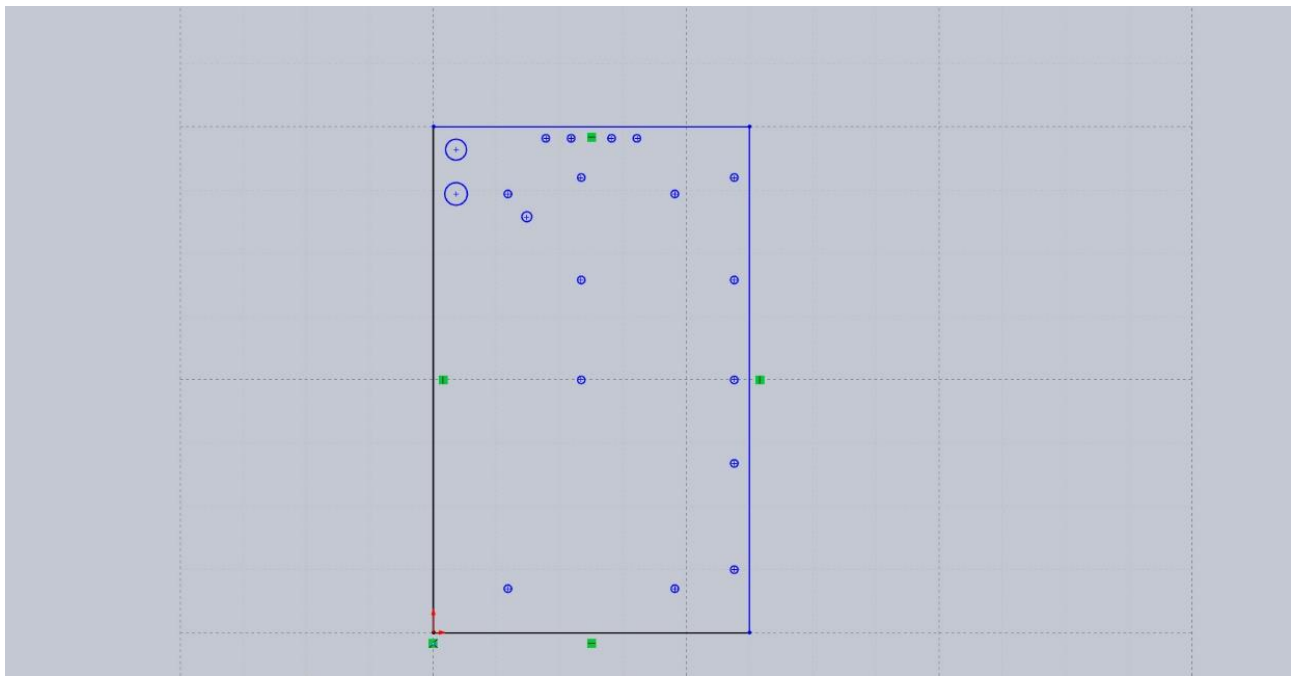


Fig. 3. Platform for the tank base.

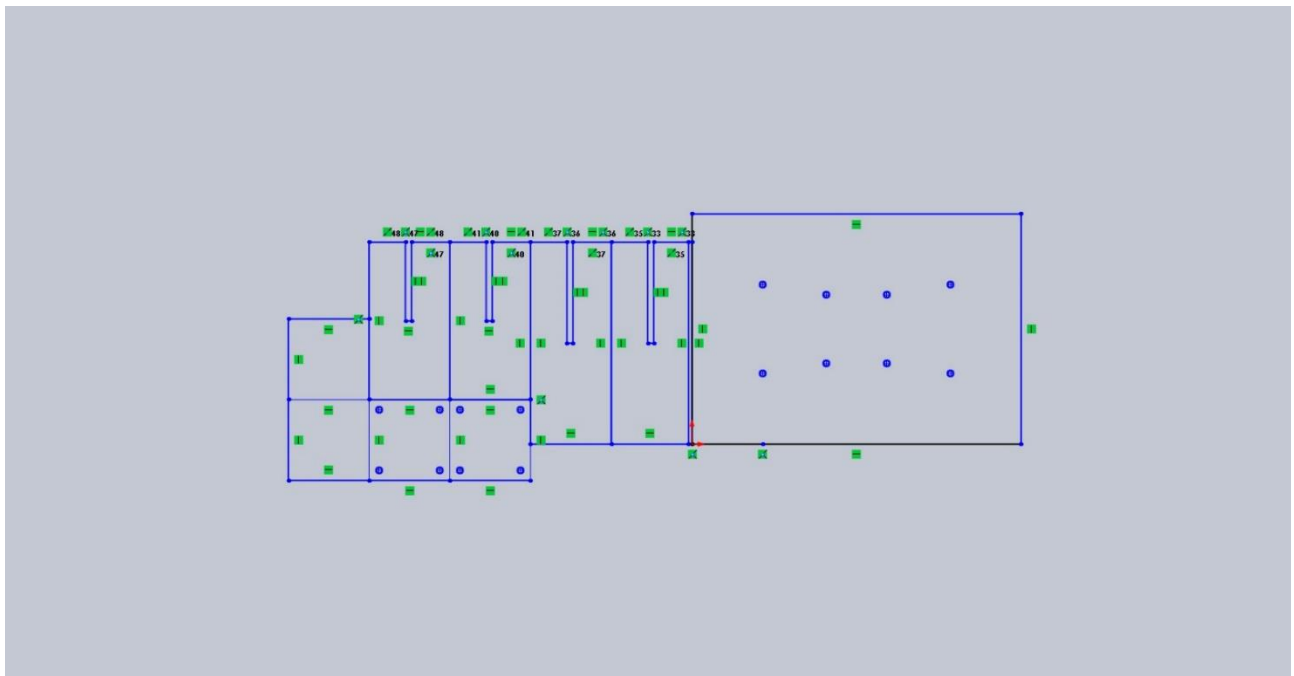


Fig. 4. Transmitter platform base and poles for transmitter and receiver boxes.

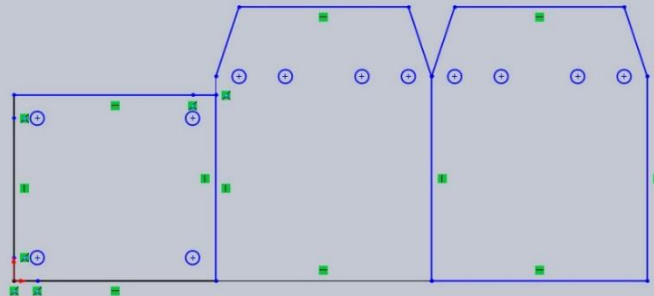


Fig. 5. Fixed pole stand for receiver box.

10. 2 APPENDIX 2: Full sized circuit diagrams

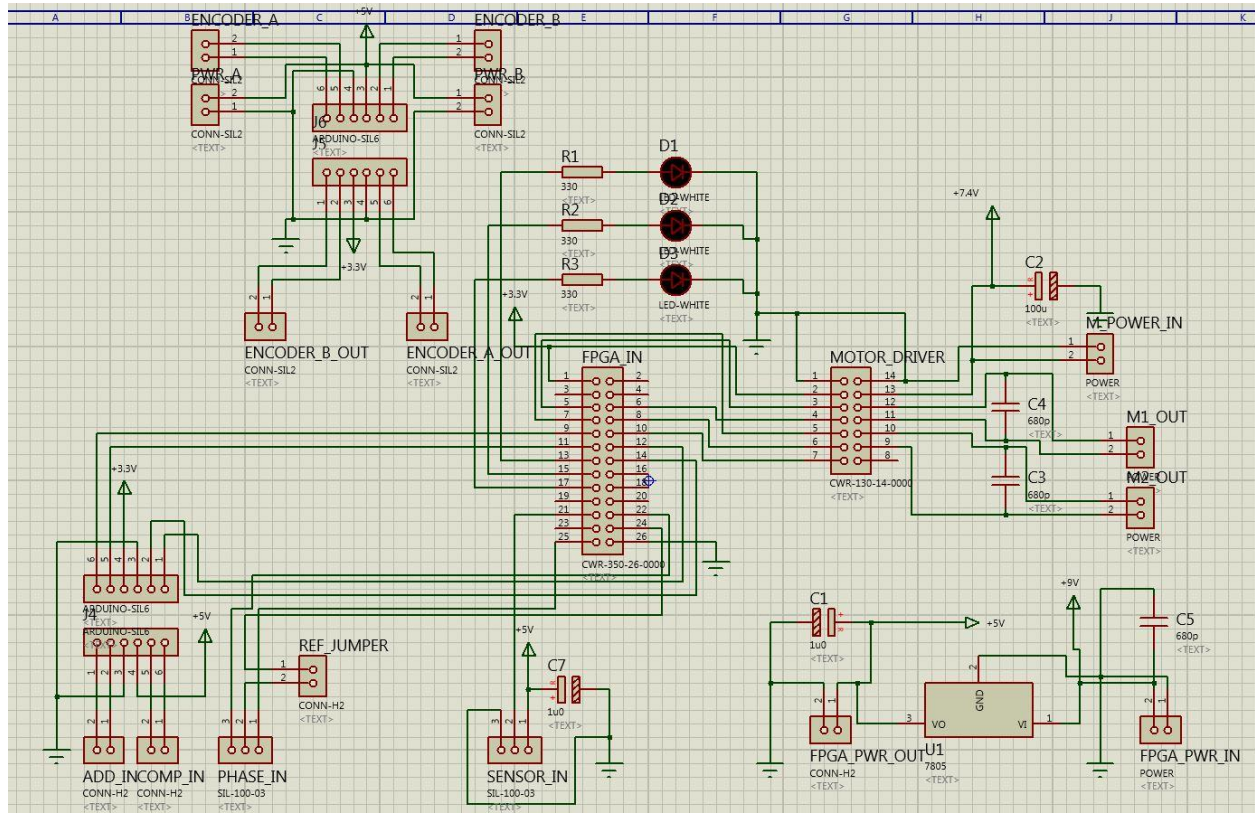


Fig. 6. Controller board circuit.

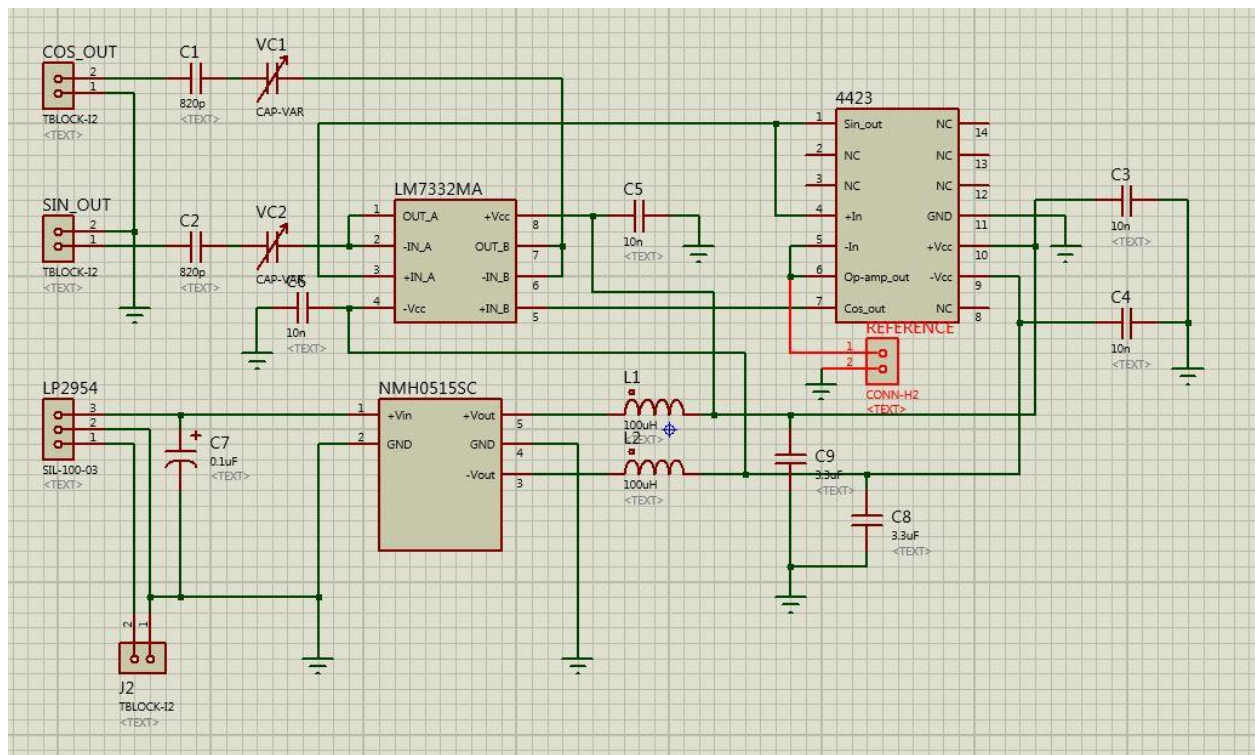


Fig. 7. Excitation circuit.

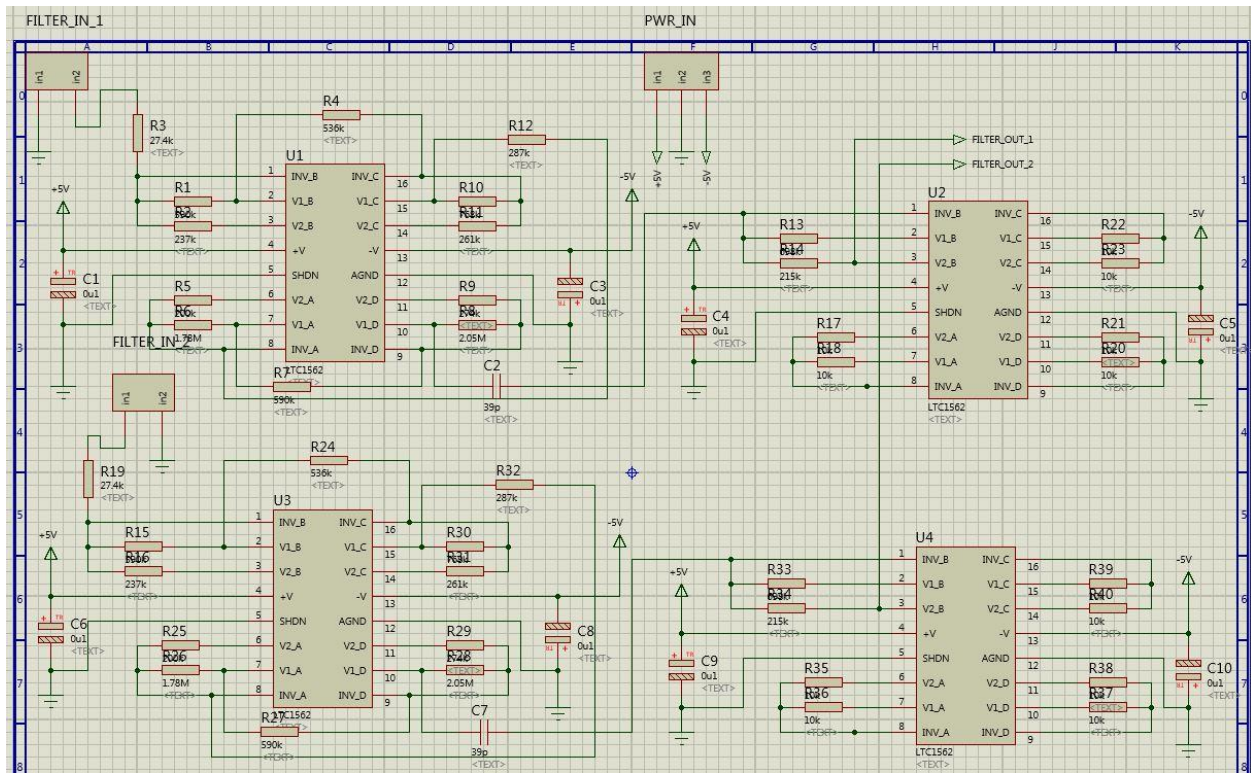


Fig. 8. Filter circuit.

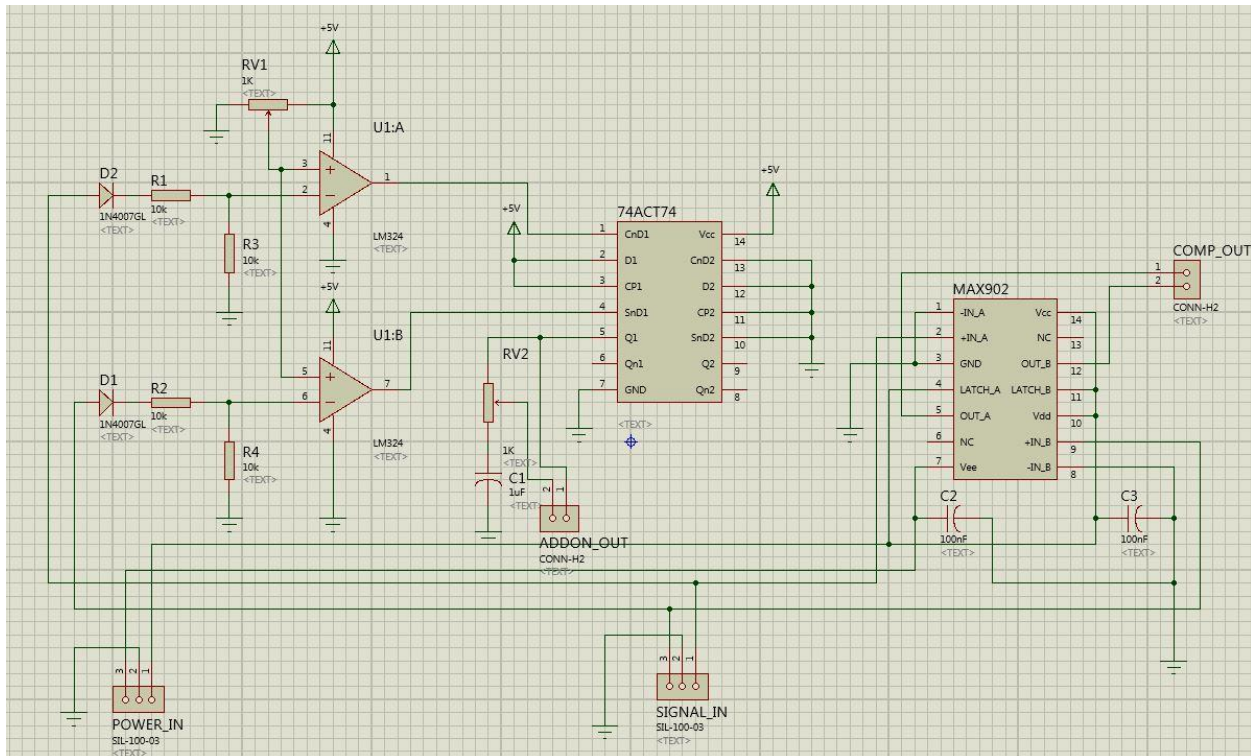


Fig. 9. Comparator circuit.

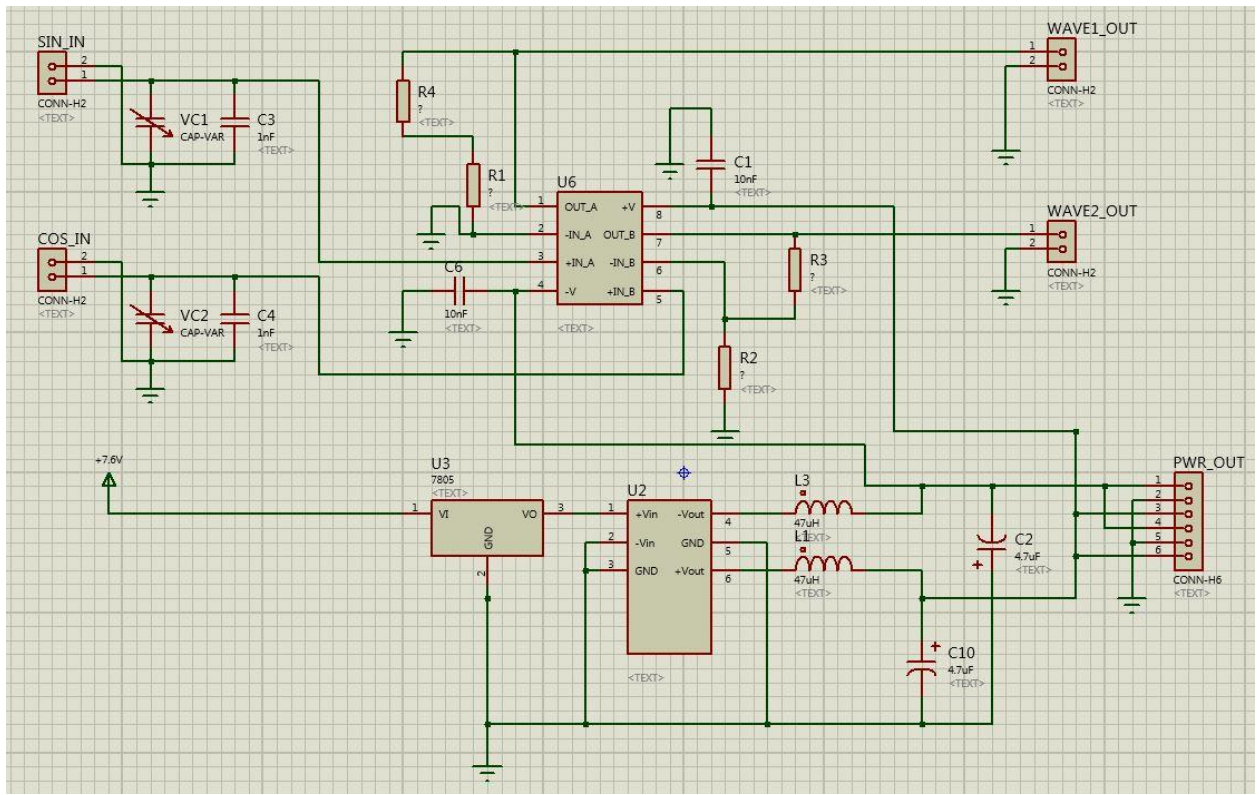


Fig. 10. Input and Power circuit.

10. 3 APPENDIX 3: Datasheets

LM7332MA - <http://pdf1.alldatasheet.com/datasheet-pdf/view/228974/NSC/LM7332.html>

LM7332 Dual Rail-to-Rail Input/Output 30V, Wide Voltage Range, High Output Operational Amplifier

General Description

The LM7332 is a dual rail-to-rail input and output amplifier with a wide operating temperature range (-40°C to $+125^{\circ}\text{C}$) which meets the needs of automotive, industrial and power supply applications. The LM7332 has the output current of 100 mA which is higher than that of most monolithic op amps. Circuit designs with high output current requirements often need to use discrete transistors because many op amps have low current output. The LM7332 has enough current output to drive many loads directly, saving the cost and space of the discrete transistors.

The exceptionally wide operating supply voltage range of 2.5V to 32V alleviates any concerns over functionality under extreme conditions and offers flexibility of use in a multitude of applications. Most of this device's parameters are insensitive to power supply variations; this design enhancement is another step in simplifying usage. Greater than rail-to-rail input common mode voltage range allows operation in many applications, including high side and low side sensing, without exceeding the input range.

The LM7332 can drive unlimited capacitive loads without oscillations.

The LM7332 is offered in the 8-pin MSOP and SOIC packages.

Features

$(V_S = \pm 15\text{V}, T_A = 25^{\circ}\text{C}$, typical values unless specified.)	
■ Wide supply voltage range	2.5V to 32V
■ Wide input common mode voltage	0.3V beyond rails
■ Output short circuit current	>100 mA
■ High output current (1V from rails)	$\pm 70\text{ mA}$
■ GBWP	21 MHz
■ Slew rate	15.2 V/ μs
■ Capacitive load tolerance	Unlimited
■ Total supply current	2.0 mA
■ Temperature range	-40°C to $+125^{\circ}\text{C}$
■ Tested at -40°C , $+125^{\circ}\text{C}$, and 25°C at 5V, $\pm 5\text{V}$, $\pm 15\text{V}$	

Applications

- MOSFET and power transistor driver
- Replaces discrete transistors in high current output circuits
- Instrumentation 4-20 mA current loops
- Analog data transmission
- Multiple voltage power supplies and battery chargers
- High and low side current sensing
- Bridge and sensor driving
- Digital to analog converter output

LP2954 – <http://www.ti.com/lit/ds/snvs096d/snvs096d.pdf>

LP2954/LP2954A 5V and Adjustable Micropower Low-Dropout Voltage Regulators

Check for Samples: LP2954, LP2954A

FEATURES

- 5V Output within 1.2% Over Temperature (A Grade)
- Adjustable 1.23 to 29V Output Voltage Available (LP2954IM and LP2954AIM)
- Ensured 250 mA Output Current
- Extremely Low Quiescent Current
- Low Dropout Voltage
- Reverse Battery Protection
- Extremely Tight Line and Load Regulation
- Very Low Temperature Coefficient
- Current and Thermal Limiting
- Pin Compatible with LM2940 and LM340 (5V Version Only)
- Adjustable Version Adds Error Flag to Warn of Output Drop and a Logic-Controlled Shutdown

APPLICATIONS

- High-Efficiency Linear Regulator
- Low Dropout Battery-Powered Regulator

Package Outline and Ordering Information

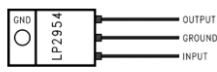


Figure 1. TO-220 3-Lead Plastic Package (Front View)

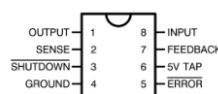


Figure 2. SO-8 Small Outline Surface Mount (Top View)



LTC1562

Very Low Noise, Low Distortion
Active RC Quad Universal Filter

FEATURES

- Continuous Time—No Clock
- Four 2nd Order Filter Sections, 10kHz to 150kHz Center Frequency
- $\pm 0.5\%$ Typical Center Frequency Accuracy
- $\pm 0.3\%$ Typical Center Frequency Accuracy (A Grade)
- Wide Variety of Response Shapes
- Lowpass, Bandpass and Highpass Responses
- 103dB Typical S/N, $\pm 5V$ Supply ($Q = 1$)
- 97dB Typical S/N, Single 5V Supply ($Q = 1$)
- 96dB Typical S/(N + THD) at $\pm 5V$ Supply, 20kHz Input
- Rail-to-Rail Input and Output Voltages
- DC Accurate to 3mV (Typ)
- “Zero-Power” Shutdown Mode
- Single or Dual Supply, 5V to 10V Total
- Resistor-Programmable f_0 , Q, Gain

APPLICATIONS

- High Resolution Systems (14 Bits to 18 Bits)
- Antialiasing/Reconstruction Filters
- Data Communications, Equalizers
- Dual or I-and-Q Channels (Two Matched 4th Order Filters in One Package)
- Linear Phase Filtering
- Replacing LC Filter Modules

DESCRIPTION

The LTC[®]1562 is a low noise, low distortion continuous-time filter with rail-to-rail inputs and outputs, optimized for a center frequency (f_0) of 10kHz to 150kHz. Unlike most monolithic filters, no clock is needed. Four independent 2nd order filter blocks can be cascaded in any combination, such as one 8th order or two 4th order filters. Each block's response is programmed with three external resistors for center frequency, Q and gain, using simple design formulas. Each 2nd order block provides lowpass and bandpass outputs. Highpass response is available if an external capacitor replaces one of the resistors. Allpass, notch and elliptic responses can also be realized.

The LTC1562 is designed for applications where dynamic range is important. For example, by cascading 2nd order sections in pairs, the user can configure the IC as a dual 4th order Butterworth lowpass filter with 94dB signal-to-noise ratio from a single 5V power supply. Low level signals can exploit the built-in gain capability of the LTC1562. Varying the gain of a section can achieve a dynamic range as high as 118dB with a $\pm 5V$ supply.

Other cutoff frequency ranges can be provided upon request. Please contact LTC Marketing.

LTC, LTC and LT are registered trademarks of Linear Technology Corporation.



Murata Power Solutions



FEATURES

- RoHS compliant
- Efficiency up to 86%
- Power density up to 1.44W/cm³
- Wide temperature performance at full 2 watt load, -40°C to 85°C
- Dual output from a single input rail
- UL 94V-0 package material
- No heatsink required
- Footprint from 1.46cm²
- Industry standard pinout
- Power sharing on output
- 1kVDC isolation
- 5V, 12V, 24V & 48V input
- 5V, 9V, 12V and 15V output
- Internal SMD construction
- Fully encapsulated with toroidal magnetics
- No external components required
- MTTF up to 1.5 million hours
- No electrolytic or tantalum capacitors

NMH Series

Isolated 2W Dual Output DC/DC Converters

Order Code	SELECTION GUIDE							Package Style
	Nominal Input Voltage	Output Voltage	Output Current	Input Current at Rated Load	Efficiency	Isolation Capacitance pF	MTTF ¹ kHrs	
NMH0505DC	5	± 5	± 200	500	80	24	1574	
NMH0509DC	5	± 9	± 111	494	81	28	663	
NMH0512DC	5	± 12	± 83	488	82	30	338	
NMH0515DC	5	± 15	± 67	476	84	33	187	
NMH0505SC	5	± 5	± 200	500	80	24	1574	
NMH0509SC	5	± 9	± 111	494	81	28	663	
NMH0512SC	5	± 12	± 83	488	82	30	338	SIP
NMH0515SC	5	± 15	± 67	476	84	33	187	
NMH1205DC	12	± 5	± 200	208	80	35	490	
NMH1209DC	12	± 9	± 111	201	83	55	343	
NMH1212DC	12	± 12	± 83	198	84	63	229	DIP
NMH1215DC	12	± 15	± 67	198	84	66	148	
NMH1205SC	12	± 5	± 200	208	80	35	490	
NMH1209SC	12	± 9	± 111	201	83	55	343	SIP
NMH1212SC	12	± 12	± 83	198	84	63	229	
NMH1215SC	12	± 15	± 67	198	84	66	148	
NMH2405DC	24	± 5	± 200	103	81	41	318	
NMH2409DC	24	± 9	± 111	98	85	75	249	
NMH2412DC	24	± 12	± 83	97	86	95	183	DIP
NMH2415DC	24	± 15	± 67	97	86	104	127	
NMH2405SC	24	± 5	± 200	103	81	41	318	
NMH2409SC	24	± 9	± 111	98	85	75	249	
NMH2412SC	24	± 12	± 83	97	86	95	183	SIP
NMH2415SC	24	± 15	± 67	97	86	104	127	
Obsolete								
NMH4805DC	48	± 5	± 200	51	82	45	235	
NMH4809DC	48	± 9	± 111	51	82	74	195	DIP
NMH4812DC	48	± 12	± 83	49	85	90	152	
NMH4815DC	48	± 15	± 67	49	85	112	112	
NMH4805SC	48	± 5	± 200	51	82	45	235	
NMH4809SC	48	± 9	± 111	51	82	74	195	SIP

Get Your Local Sales Rep

Precision Quadrature Oscillator

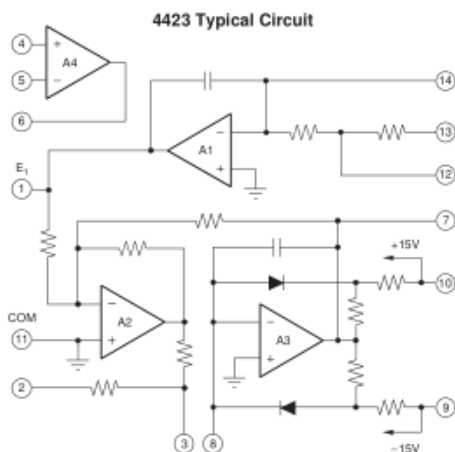
FEATURES

- Sine and Cosine Outputs
- Resistor-Programmable Frequency
- Wide Frequency Range: 0.002Hz to 20kHz
- Low Distortion: 0.2% max up to 5kHz
- Easy Adjustments
- Small Size
- Low Cost

DESCRIPTION

The Model 4423 is a precision quadrature oscillator. It has two outputs 90 degrees out of phase with each other, thus making sine and cosine wave outputs available at the same time. The 4423 is resistor-programmable and is easy to use. It has low distortion (0.2% max up to 5kHz) and excellent frequency and amplitude stability.

The Model 4423 also includes an uncommitted operational amplifier that may be used as a buffer, level shifter, or as an independent operational amplifier. The 4423 is packaged in a versatile, small, low-cost DIP package.



DUAL LOW VOLTAGE H-BRIDGE IC

Check for Samples: [DRV8835](#)

FEATURES

- Dual-H-Bridge Motor Driver
 - Capable of Driving Two DC Motors or One Stepper Motor
 - Low MOSFET On-Resistance: HS + LS 305 mΩ
- 1.5-A Maximum Drive Current Per H-Bridge
- Bridges May Be Paralleled for 3-A Drive Current
- Separate Motor and Logic Supply Pins:
 - 0-V to 11-V Motor-Operating Supply-Voltage Range
 - 2-V to 7-V Logic Supply-Voltage Range
- Separate Logic and Motor Power Supply Pins
- Flexible PWM or PHASE/ENABLE Interface
- Low-Power Sleep Mode With 95-nA Maximum Supply Current
- Tiny 2-mm x 3-mm WSON Package

APPLICATIONS

- Battery-Powered:
 - Cameras
 - DSLR Lenses
 - Consumer Products
 - Toys
 - Robotics
 - Medical Devices

DESCRIPTION

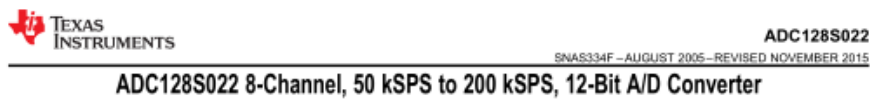
The DRV8835 provides an integrated motor driver solution for cameras, consumer products, toys, and other low-voltage or battery-powered motion control applications. The device has two H-bridge drivers, and can drive two DC motors or one stepper motor, as well as other devices like solenoids. The output driver block for each consists of N-channel power MOSFET's configured as an H-bridge to drive the motor winding. An internal charge pump generates needed gate drive voltages.

The DRV8835 can supply up to 1.5-A of output current per H-bridge. It operates on a motor power supply voltage from 0 V to 11 V, and a device power supply voltage of 2 V to 7 V.

PHASE/ENABLE and IN/IN interfaces can be selected which are compatible with industry-standard devices.

Internal shutdown functions are provided for over current protection, short circuit protection, under voltage lockout and overtemperature.

The DRV8835 is packaged in a tiny 12-pin WSON package with PowerPAD™ (Eco-friendly: RoHS & no Sb/Br).



1 Features

- Eight Input Channels
- Variable Power Management
- Independent Analog and Digital Supplies
- SPI™/QSPI™/MICROWIRE/DSP Compatible
- Packaged in 16-lead TSSOP
- Conversion Rate: 50 kps to 200ksp
- DNL ($V_A = V_D = 5$ V): $\pm 1 / -0.7$ LSB (Maximum)
- INL ($V_A = V_D = 5$ V): ± 1 LSB (Maximum)
- Power Consumption
 - 3V Supply: 1.2 mW (Typical)
 - 5V Supply: 7.5 mW (Typical)

2 Applications

- Automotive Navigation
- Portable Systems
- Medical Instruments
- Mobile Communications
- Instrumentation and Control Systems

3 Description

The ADC128S022 device is a low-power, eight-channel CMOS 12-bit analog-to-digital converter specified for conversion throughput rates of 50 kps to 200 kps. The converter is based on a successive-approximation register architecture with an internal track-and-hold circuit. It can be configured to accept up to eight input signals at inputs IN0 through IN7.

The output serial data is straight binary and is compatible with several standards, such as SPI, QSPI, MICROWIRE, and many common DSP serial interfaces.

The ADC128S022 may be operated with independent analog and digital supplies. The analog supply (V_A) can range from 2.7 V to 5.25 V, and the digital supply (V_D) can range from 2.7 V to V_A . Normal power consumption using a 3-V or 5-V supply is 1.2 mW and 7.5 mW, respectively. The power-down feature reduces the power consumption to 0.06 μ W using a 3-V supply and 0.25 μ W using a 5-V supply.

The ADC128S022 is packaged in a 16-lead TSSOP package. Operation over the extended industrial temperature range of -40°C to $+105^{\circ}\text{C}$ is ensured.

Device Information⁽¹⁾

PART NUMBER	PACKAGE	BODY SIZE (NOM)
ADC128S022	TSSOP (16)	4.40 mm \times 5.00 mm

⁽¹⁾ For all available packages, see the orderable addendum at the end of the data sheet.

The DE0-Nano board introduces a compact-sized FPGA development platform suited for a wide range of portable design projects, such as robots and mobile projects.

The DE0-Nano is ideal for use with embedded soft processors—it features a powerful Altera Cyclone IV FPGA (with 22,320 logic elements), 32 MB of SDRAM, 2 Kb EEPROM, and a 64 Mb serial configuration memory device. For connecting to real-world sensors the DE0-Nano includes a National Semiconductor 8-channel 12-bit A/D converter, and it also features an Analog Devices 13-bit, 3-axis accelerometer device.

The DE0-Nano board includes a built-in USB Blaster for FPGA programming, and the board can be powered either from this USB port or by an external power source. The board includes expansion headers that can be used to attach various Terasic daughter cards or other devices, such as motors and actuators. Inputs and outputs include 2 pushbuttons, 8 user LEDs and a set of 4 dip-switches.

1.1 Features

Figure 1-1 shows a photograph of the DE0-Nano Board.



Figure 1-1 The DE0-Nano Board

BSS138 Transistor – <http://cdn.sparkfun.com/datasheets/BreakoutBoards/BSS138.pdf>

BSS138

N-Channel Logic Level Enhancement Mode Field Effect Transistor

General Description

These N-Channel enhancement mode field effect transistors are produced using Fairchild's proprietary, high cell density, DMOS technology. These products have been designed to minimize on-state resistance while provide rugged, reliable, and fast switching performance. These products are particularly suited for low voltage, low current applications such as small servo motor control, power MOSFET gate drivers, and other switching applications.

Features

- 0.22 A, 50 V. $R_{DS(on)} = 3.5\Omega @ V_{GS} = 10\text{ V}$
 $R_{DS(on)} = 6.0\Omega @ V_{GS} = 4.5\text{ V}$
- High density cell design for extremely low $R_{DS(on)}$
- Rugged and Reliable
- Compact industry standard SOT-23 surface mount package



Absolute Maximum Ratings $T_A=25^\circ\text{C}$ unless otherwise noted

Symbol	Parameter	Ratings	Units
V_{DSS}	Drain-Source Voltage	50	V
V_{GSS}	Gate-Source Voltage	± 20	V
I_D	Drain Current – Continuous – Pulsed	0.22 0.88	A
P_D	Maximum Power Dissipation <small>(Note 1)</small> Derate Above 25°C	0.36 2.8	mW/ $^\circ\text{C}$
T_A, T_{STO}	Operating and Storage Junction Temperature Range	-55 to +150	$^\circ\text{C}$
T_L	Maximum Lead Temperature for Soldering Purposes, 1/16" from Case for 10 Seconds	300	$^\circ\text{C}$

Rover 5 – <http://www.dfrobot.com/image/data/ROB0055/Rover%205%20Introduction.pdf>

ROVER 5



Rover 5 is a new breed of tracked robot chassis designed specifically for students and hobbyist. Unlike conventional tracked chassis's the clearance can be adjusted by rotating the gearboxes in 5-degree increments. "Stretchy" rubber treads maintain tension as the clearance is raised.

Maisto Tech RC Radio Controlled Rock Crawler - <https://www.amazon.co.uk/Maisto-Tech-Radio-Controlled-Crawler/dp/B003DKO2EY>



10.4 APPENDIX 4: Project materials and cost full graph

Project items and costs							
Item description	Source	Required quantity	Price	Quantity ordered	Total	Sum for each category	Grand total
Power and input circuit						21.54	332.129
DC/DC Converter NMH0505SC +5V/-5V	Farnell	1	6.34	1	6.34		
LM7332 amplifier	Farnell	1	4.19	1	4.19		
4.7 µF, ± 20%	Farnell	2	2.89	2	5.78		
47UH, 10%	Farnell	2	0.504	3	1.51		
10nF capacitor	Farnell	2	0.255	2	0.51		
LP2954IT Voltage regulator 5V	Farnell	1	2.41	1	2.41		
50pF variable capacitor 3 pin package	Store	2	0.26	2	0.52		
0.1uF 2mm pitch capacitor electrolytic	Store	1	0.07	2	0.14		
Resistors (input divider and gain adjustment)	Store	4	0	4	0		
680pf ceramic capacitor (2.5mm pitch)	Store	2	0.07	2	0.14		
PCB Production	Store	1	2.9	1	2.9		
Filter circuit						49.108	
27.4k	Farnell	2	0.595	4	2.38		
536k	Farnell	2	0.604	4	2.416		
590k	Farnell	4	0.548	4	2.192		
237k	Farnell	2	0.62	4	2.48		
0.1uF	Farnell	4	0.13	6	0.78		
200k	Farnell	2	0.608	4	2.432		
1.78M (1.6M part) in series	Farnell	2	0.067	10	0.67		
1.78M (180k part) in series	Farnell	2	0.447	5	2.235		
287k	Farnell	2	0.57	10	5.7		
768k	Farnell	2	0.118	10	1.18		
261k	Farnell	2	0.06	10	0.6		
274k	Farnell	2	0.56	10	5.6		
2.05M (2M part) in series	Farnell	2	0.058	10	0.58		
2.05M (50k part) in series	Farnell	2	0.857	5	4.285		
39pF	Farnell	2	1.11	2	2.22		
698k (680k part) in series	Farnell	2	0.0415	10	0.415		
698k (18k part) in series	Farnell	2	0.058	10	0.58		
215k	Farnell	2	0.057	4	0.228		
10k	Farnell	12	0.529	15	7.935		
PCB Production	Store	4.2	1	4.2	4.2		
Transmitter circuit/platform						31.286	
4423 Quadrature oscillator	Ebay	1	10.65	1	10.65		
DC/DC Converter NMH0515SC 15/-15v	Farnell	1	6.34	1	6.34		
LM7332 amplifier	Farnell	1	4.19	1	4.19		
LP2954IT Voltage regulator 5V	Farnell	1	2.41	1	2.41		
100uH 2mm pitch inductor	Rs-online	2	0.242	2	0.484		
3.3uF 2.54mm pitch ceramic capacitor	Rs-online	2	0.996	2	1.992		
0.1uF 2mm pitch capacitor electrolytic	Store	1	0.07	2	0.14		
50pF variable capacitor 3 pin package	Store	2	0.26	2	0.52		
680pf ceramic capacitor (2.5mm pitch)	Store	2	0.07	2	0.14		
10nf polyester capacitor (5mm pitch)	Store	4	0.03	4	0.12		
PCB Production	Store	1	4.3	1	4.3		
Comparator circuit						26.259	
10k variable resistor	Ebay	2	0.468	5	2.34		
CD74ACT74E	Farnell	1	0.21	2	0.42		
LM324N	Farnell	1	0.401	2	0.802		
2.2k	Farnell	4	0.0546	10	0.546		
1N4007	Farnell	2	0.106	4	0.424		
0.1uF decoupling capacitor	Farnell	1	0.267	7	1.869		
1uF capacitor	Farnell	4	0.493	6	2.958		
MAX902EPD+	Farnell	1	11.09	1	11.09		
10nF capacitor	Farnell	2	0.255	2	0.51		
PCB Production	Store	2	5.3	1	5.3		
Controller board						75.15	
4-Channel logic level shifter	Ebay	2	1.89	2	3.78		
Pololu DRV8835 Dual Motor Driver Carrier	Ebay	1	7.11	0	0		
LP2954IT Voltage regulator 5V	Farnell	1	2.41	1	2.41		
10nF ceramic capacitor	Farnell	2	0.255	2	0.51		
EP4CE22F17C6N DEO-NANO FPGA	Store	1	63.34	1	63.34		
3300ohm resistors for LEDs	Store	3	0	3	0		
Screw terminal block 2 pin (5mm pitch)	Store	2	0.07	2	0.14		
Single header terminal 36 pins	Store	1	0.07	1	0.07		
PCB Production	Store	1	4.9	1	4.9		
Additional components						128.786	
RC Controlled truck	Amazon	1	16.56	1	16.56		
8 x 1.5v battery holder	Amazon	1	1.19	2	2.38		
Rover 5 Tank Kit and Microcontroller	DFRobot	1	69.7	1	69.7		
Copper tape for shielding	Ebay	1	3.59	1	3.59		
Micro JST 2.0 PH 2-Pin Connector plug with Wires	Ebay	5	0.109	10	1.09		
5.5mm Bullet Connector Power Charge Cable	Ebay	1	8.29	1	8.29		
0.16mm Coil for transmitter 100g	Ebay	1	4.25	1	4.25		
0.10mm Coil for receiver 125g	Ebay	1	5.95	1	5.95		
JST connector 15cm 3 pin	Ebay	1	0.121	10	1.21		
Indicator 1-8s RC Lipo Battery Voltage Tester	Ebay	2	1.59	2	3.18		
26 way female header (DEO-NANO connection)	Ebay	1	1.77	1	1.77		
DESOLDERING BRAID	Farnell	1	6.32	1	6.32		
Screw terminal block 2 pin (2.54mm pitch)	Farnell	4	0.459	4	1.836		
Jumper wires	Farnell	4	0.149	10	1.49		
Headers	Farnell	4	0.103	10	1.03		
Screw terminal block 2 pin (5mm pitch)	Store	2	0.07	2	0.14		
Unused components						0.96	
7805 voltage regulator	Store	2	0.16	2	0.32		
4.7uf tantalum capacitor (5mm pitch)	Store	1	0.16	4	0.64		

10.5 APPENDIX 5: Final result

